Renewable and Sustainable Energy Reviews 37 (2014) 69–89

Contents lists available at ScienceDirect

Renewable and Sustainable Energy Reviews

journal homepage: www.elsevier.com/locate/rser

A novel voltage and frequency controller for standalone DFIG based Wind Energy Conversion System

Rishabh Dev Shukla*, Ramesh Kumar Tripathi

Department of Electrical Engineering, M N National Institute of Technology Allahabad, India

ARTICLE INFO

Article history:
Received 27 July 2013
Received in revised form
5 April 2014
Accepted 27 April 2014
Available online 27 May 2014

Keywords:
Doubly fed induction generator (DFIG)
Stand-alone generation
RSC
Root mean square detection
Voltage and frequency controller

ABSTRACT

This paper presents a new speed-sensorless control strategy for a stand-alone doubly-fed induction generator supplying energy to an isolated load. The method is based on the root mean square (rms) detection scheme. The generated stator voltage is controlled via rotor currents. Amplitude of stator voltage and its frequency are controlled simultaneously. The output signals from the voltage controllers are the reference signals for the rotor current amplitude and frequency of the stator voltage is regulated with the help of frequency control loop. This developed direct voltage control method is applicable for both the balanced and unbalanced load and also for standalone and grid connected mode. The control pulses for the rotor side converter is supplied by the hysteresis controller which is operated on the error signal calculated between actual and reference rotor currents. This paper also provides the brief idea about the voltage and frequency control on modern Autonomous DFIG based Wind Energy Systems via single phase mathematical model of standalone DFIG system. A short state-of-the-art review on mechanical position/speed sensorless control schemes for autonomous DFIG based WESs is presented, which helps the present researcher and students working in this area. These include stator flux oriented control techniques; direct voltage control techniques; MARS observer based techniques for autonomous DFIG-based variable-speed WESs. Simulation results obtained from a 2MVA DFIG system, prototype in MATLab/Simulink, are presented and discussed in this paper.

Contents

1. Introduction

From the past two decades, wind energy is a very crucial renewable energy source. In earlier period, the technology used in WECS was based on squirrel-cage induction generators (SCIG), running at constant speed, directly connected to grid, Fig. 1(a). The fixed speed Wind Energy Conversion Systems (WECSs) employ a number of gearbox stages operate only in a narrow range around the

* Corresponding author. Visiting faculty, Department of Electrical Engineering, Motilal Nehru National Institute of Technology Allahabad, Uttar Pradesh, India-211004.
E-mail addresses: shukla.rishabhdev@gmail.com, rishudev1984@gmail.com (R.D. Shukla).

http://dx.doi.org/10.1016/j.rser.2014.04.069
1364-0321/

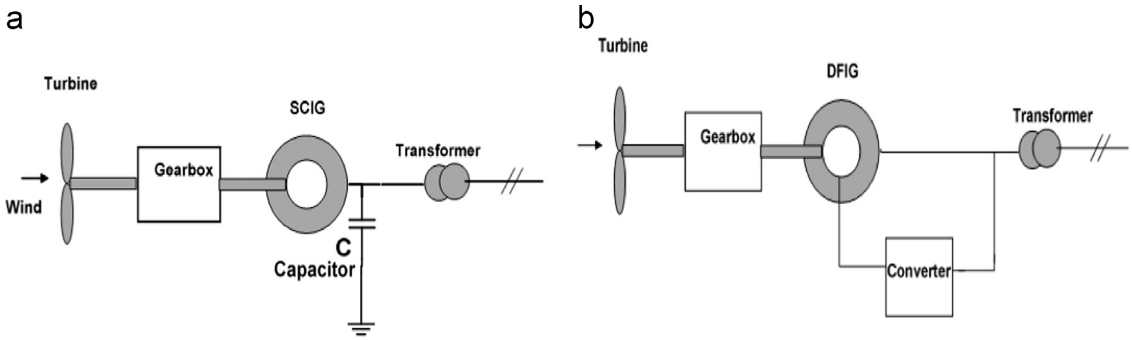


Fig. 1. (a) Scheme of a fixed speed concept with SCIG system and (b) scheme of a variable speed concept with DFIG system.

synchronous speed, always draws reactive power from the grid are directly connected to the grid through a transformer [1]. Presently, the technology moves towards variable speed WECS. Also the controlling of the WESC becomes very important as the power level increases. The variable speed WECSs have been used with an arrangement is well-known as the DFIG concept, Fig. 1(b), which belongs to a variable speed wind turbine with a wound rotor induction generator and power electronics converter on the rotor side.

This concept gives a wide speed operational range, depending on the size of the power electronics converter. Typically, the speed ranges from +30% to −30% around the synchronous speed [2]. The rating of the power electronic converter is only 25–30% of the generator capacity, which makes this concept attractive and popular from an economic point of view [3]. A number of publications and research works have been reported on the grid connected operation of DFIG based WECSs [3–10]. The grid connected DFIG based WECS is comparatively older and is extensively used today. However, scanty attention has been paid toward the issues of stand-alone DFIG based WECSs. In case, the users are at a distant away from the grid and cannot use the energy provided by grid, a stand-alone generating system can be used. A stand-alone generating system must be capable to supply the users with regulated voltage and frequency [13,14,23]. In these cases, wound rotor induction machine (WRIM) offers more useful characteristics working at variable speed while regulating the generated voltage and frequency [13–43]. The stand alone and the grid connected operation of the DFIG based WECS is very different to each other and needs different controllers. There are only some techniques in the literature about the speed-sensorless control of the slip-ring machines [3,50]. But, these techniques will not be discussed in this paper because they associated to the grid connected mode of operation. In grid connected mode, active and reactive powers are controlled, which results in failure to regulate output voltage and frequency in stand-alone mode. It makes the WECS useless after the grid outage; thus, the control techniques for stator voltage amplitude and frequency control were developed. A method described in [37] is only one recognized sensorless control for stand-alone DFIG. The predicted speed is given by synchronization of predicted and measured stator flux, with stator flux estimation related to the stator and rotor currents. To control the amplitude of the stator voltage, a magnetizing current control is used. The assumption is that the magnetizing current is applied only from the rotor side. But it is true only for resistive load [25]. It was tested only for resistive load. Also the high-frequency harmonics in stator voltage, produced by pulse width modulation converter, are limited (by reducing the rotor current ripples) by the additional extremely large chokes connected to the rotor. The given method is based on the flux control rather than a stator voltage control. The flux and voltage are sinusoidal in case of linear load; but, in the case of nonlinear load, stator voltage is distorted more than flux, and these additional distortions are not completely taken into account during the flux control method. Therefore, another technique is presented by Iwanski and Koczara in [18–32]. It is sensorless direct voltage control technique. The method uses a phase-locked loop (PLL) for the synchronization of the actual output voltage vector with the reference vector. The method based on the stator voltage vector control represented in the synchronously rotated polar coordinates. The generated stator/load voltage is controlled by rotor currents. Amplitude of stator voltage and its frequency are controlled separately. The method is applicable for both the stand alone and the grid connected operation.

There are two basic methods of standalone generator voltage control: stator flux oriented control [12–16] and direct voltage control (DVC) [18–32]. The direct voltage control DVC is much simpler than the stator flux oriented control. In the DVC control, any information from mechanical sensors or estimators on the rotor speed or position angle is not needed. In [23,25], the authors proposed dq0 transformation to regulate output or stator voltages and need to tune the two PI controllers. For unbalance loads, extended method is given [24–26], which uses positive and negative sequence controllers, but this needs lots of calculation. So in this paper, a novel control strategy to control the voltage and frequency of a WRIM working as a variable speed stand-alone generating system supplying a balance and unbalanced *R–L* load is proposed. This technique based on the root mean square (rms) detection. The control of load side converter is beyond the scope of this paper and only a diode rectifier is used for the purpose. Because the stand-alone system requires initial energy for excitation, so here a dc battery is connected for short duration of time and after that filtering capacitors are solving this problem. Here we need one (for balanced load) and three (for unbalanced load) PI controllers for each of the three phases. This proposed technique is simple and easy to implement than any other technique used for control of voltage and frequency in standalone DFIG based WECS. This paper is organized as follows: Section 2 discusses the basics of wind turbine concept with the modeling of standalone DFIG based WECS and a short state-of-the-art review on mechanical position/speed sensorless control schemes for standalone DFIG based WESs is presented, these include stator flux oriented control techniques; direct voltage control techniques; MARS observer based techniques for autonomous DFIG-based variable-speed WESs. Section 3 discusses the proposed technique for voltage and frequency control of the stator voltage. Section 4 presents the simulation results with their discussions. Section 5 presents the conclusions and future scope.

2. Standalone DFIG based WECS

The power generated by a WT can be expressed as [11,53]

$$P = 0.5\rho\pi R^2 V^3 C_P(\lambda, \beta) \quad (1)$$

where ρ is the air density in kg/m^3, R the turbine rotor radius, V the wind speed, and C_p is the turbine power coefficient that represents the power conversion efficiency of a wind turbine. The

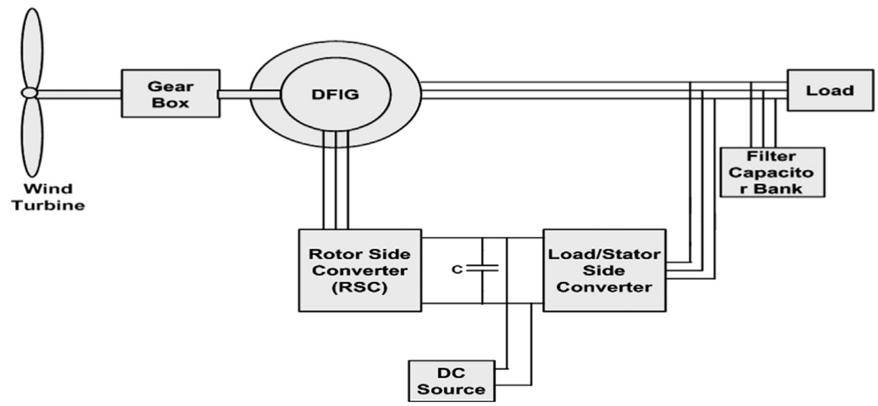


Fig. 2. Stand-alone DFIG based Wind Energy Conversion System supported by dc coupled additional power source.

physical meaning of the C_p curve is the ratio of the actual power delivered by the turbine and the theoretical power available in the wind. C_p is a function of the tip speed ratio (TSR), λ, as well as the blade pitch angle (β) in a pitch controlled wind turbine. λ is given by $\lambda = R\omega_r/V$, where ω_r is the rotational speed of the wind turbine. C_p (theoretical)$=16/27$, is the maximum theoretically possible turbine power coefficient. In practice, it is 40–45%. During high wind velocity, active pitch angle control is used to decrease the aerodynamic power by turning the rotor blades through some angle from the direction of wind. The aerodynamic power captured by the wind turbine is the cosine function of pitch angle [11]. In this paper, the pitch angle is kept zero, which is a valid supposition for lower to medium wind velocities. DFIG based wind turbine technology uses the gear box to convert low speed to high speed of rotor shaft which must be acceptable for the DFIG. In standalone DFIG based WECS, stator is not connected to the grid but supplies the isolated load. Fig. 2 illustrates the block diagram of a stand-alone DFIG based WECS supplied to an isolated load.

The rotor is connected to the load through power electronics converters. The bidirectional power flow ability is possible by the use of back-to-back voltage source converters with a common capacitive dc link. The converters are known as the rotor side converter and load side converter. The basic equation for describing the DFIG system in synchronously rotating reference frame is as follows [2,3]:

$$v_s = R_s i_s + \frac{d\lambda_s}{dt} + j\omega_s \lambda_s \tag{2}$$

$$v_r = R_r i_r + \frac{d\lambda_r}{dt} + j(\omega_s - p_b\omega_m)\lambda_r \tag{3}$$

$$\lambda_s = L_s i_s + L_m i_r \tag{4}$$

$$\lambda_r = L_r i_r + L_m i_s \tag{5}$$

where stator and rotor voltages are v_s and v_r, stator and rotor fluxes are λ_s and λ_r and stator and rotor currents are i_s and i_r, stator and rotor resistances and inductances are r_s, r_r and L_s, L_r. The mathematical model of a standalone operated DFIG is based on the same equations as the grid connected system (Eqs. (1)–(4)). Model of the grid connected DFIG with dq components of the stator and rotor currents as the state variables are described as [53]

$$\begin{bmatrix} \frac{di_{ds}}{dt} \\ \frac{di_{qs}}{dt} \\ \frac{di_{dr}}{dt} \\ \frac{di_{qr}}{dt} \end{bmatrix} = \begin{bmatrix} \frac{-R_sL_r}{L_sL_r-L_m^2} & \left(\omega_s + \frac{-\omega_m L_m^2}{L_sL_r-L_m^2}\right) & \frac{R_rL_m}{L_sL_r-L_m^2} & \frac{\omega_m L_m L_r}{L_sL_r-L_m^2} \\ -\left(\omega_s + \frac{-R_sL_r}{L_sL_r-L_m^2}\right) & \frac{-R_sL_r}{L_sL_r-L_m^2} & \frac{\omega_m L_m L_r}{L_sL_r-L_m^2} & \frac{R_rL_m}{L_sL_r-L_m^2} \\ \frac{R_sL_m}{L_sL_r-L_m^2} & -\frac{\omega_m L_m L_s}{L_sL_r-L_m^2} & \frac{-R_rL_s}{L_sL_r-L_m^2} & \left(\omega_s - \frac{\omega_m L_s L_r}{L_sL_r-L_m^2}\right) \\ \frac{\omega_m L_m L_s}{L_sL_r-L_m^2} & \frac{R_sL_m}{L_sL_r-L_m^2} & -\left(\omega_s - \frac{\omega_m L_s L_r}{L_sL_r-L_m^2}\right) & \frac{-R_rL_s}{L_sL_r-L_m^2} \end{bmatrix}$$

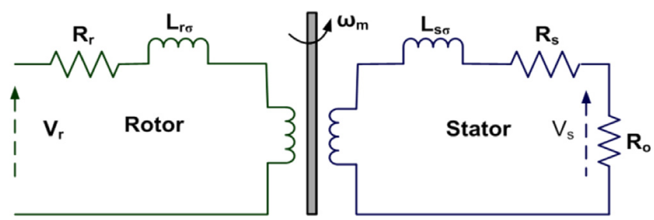


Fig. 3. Per phase equivalent circuit of DFIG supplied through rotor side with load resistance R_o.

$$\begin{bmatrix} i_{ds} \\ i_{qs} \\ i_{dr} \\ i_{qr} \end{bmatrix} + \begin{bmatrix} \frac{L_r}{L_sL_r-L_m^2} & 0 & -\frac{L_m}{L_sL_r-L_m^2} & 0 \\ 0 & \frac{L_r}{L_sL_r-L_m^2} & 0 & -\frac{L_m}{L_sL_r-L_m^2} \\ -\frac{L_m}{L_sL_r-L_m^2} & 0 & \frac{L_s}{L_sL_r-L_m^2} & 0 \\ 0 & -\frac{L_m}{L_sL_r-L_m^2} & 0 & \frac{L_s}{L_sL_r-L_m^2} \end{bmatrix} \begin{bmatrix} v_{ds} \\ v_{qs} \\ v_{dr} \\ v_{qr} \end{bmatrix} \tag{6}$$

In the case of standalone DFIG system, stator voltage is not given by the power grid, but is obtained as a consequence of the excited machine loaded on the stator side. The stator voltage during a resistive load supply is calculated as

$$v_s = -R_o i_s \tag{7}$$

where R_o is the load resistance and the stator current also represents the load current.

Now from above two equations a model of a standalone DFIG loaded with resistive load and stator and rotor current components as state variable, is given as

$$\begin{bmatrix} \frac{di_{ds}}{dt} \\ \frac{di_{qs}}{dt} \\ \frac{di_{dr}}{dt} \\ \frac{di_{qr}}{dt} \end{bmatrix} = \begin{bmatrix} \frac{-(R_s+R_o)L_r}{L_sL_r-L_m^2} & \left(\omega_s + \frac{-\omega_m L_m^2}{L_sL_r-L_m^2}\right) & \frac{R_rL_m}{L_sL_r-L_m^2} & \frac{\omega_m L_m L_r}{L_sL_r-L_m^2} \\ -\left(\omega_s + \frac{-R_sL_r}{L_sL_r-L_m^2}\right) & \frac{-(R_s+R_o)L_r}{L_sL_r-L_m^2} & -\frac{\omega_m L_m L_r}{L_sL_r-L_m^2} & \frac{R_rL_m}{L_sL_r-L_m^2} \\ \frac{(R_s+R_o)L_m}{L_sL_r-L_m^2} & \frac{-\omega_m L_m L_s}{L_sL_r-L_m^2} & \frac{-R_rL_s}{L_sL_r-L_m^2} & \left(\omega_s - \frac{\omega_m L_s L_r}{L_sL_r-L_m^2}\right) \\ \frac{\omega_m L_m L_s}{L_sL_r-L_m^2} & \frac{(R_s+R_o)L_m}{L_sL_r-L_m^2} & -\left(\omega_s - \frac{\omega_m L_s L_r}{L_sL_r-L_m^2}\right) & \frac{-R_rL_s}{L_sL_r-L_m^2} \end{bmatrix}$$

$$\begin{bmatrix} i_{ds} \\ i_{qs} \\ i_{dr} \\ i_{qr} \end{bmatrix} + \begin{bmatrix} -\frac{L_m}{L_sL_r-L_m^2} & 0 \\ 0 & -\frac{L_m}{L_sL_r-L_m^2} \\ \frac{L_s}{L_sL_r-L_m^2} & 0 \\ 0 & \frac{L_s}{L_sL_r-L_m^2} \end{bmatrix} \begin{bmatrix} v_{dr} \\ v_{qr} \end{bmatrix} \tag{8}$$

The per phase equivalent circuit model of DFIG supplied through rotor side is shown in Fig. 3 where R_o represents the load resistance. In a basic model, DFIG can be taken as a machine fed from a current source from the rotor side. The rotor is fed from VSI controlled by a current, which can be treated as current source, thus Eqs. (3) and (5) can be ignored.

From Eqs. (2) and (4) and with a resistive load and neglected stator resistance the dependence of the rotor current on the stator voltage represented in dq frame can be described by (9) [29]

$$v_s = \frac{R_o L_m}{Z_s}\frac{di_r}{dt} + j\left(\frac{\omega_s R_o L_m}{Z_s}\right) i_r - \frac{L_s}{Z_s}\frac{dv_s}{dt} \tag{9}$$

where R_o is the load resistance, stator resistance is neglected and Z_s is the stator side impedance $Z_s = R_o + j\omega_s L_s$. For an unloaded system, we have

$$v_s = L_m \frac{di_r}{dt} + j\omega_s L_m i_r \tag{10}$$

A few speed sensorless techniques about the voltage and frequency control in autonomous DFIG based wind energy system are present in the literature: stator flux oriented techniques [12–17]; direct voltage control techniques [18–32]; MARS observer based techniques [35–54]. These above techniques have their own advantages and disadvantages. But in terms of complexity, these techniques are very complex when we implement in software and/or hardware.

2.1. Indirect/stator flux oriented control technique

An indirect voltage and frequency control achieved by controlling the stator flux while neglecting the stator resistance and imposing slip frequency to the rotor currents through an algebraic relationship. Using an algebraic relationship to calculate the stator flux, based on the stator and rotor currents, can be considered to estimate the stator flux using an open loop observer. The load voltage is maintained at constant frequency and its magnitude is regulated through control of the stator flux of the generator. Estimated speed is given by synchronization of predicted and measured stator flux, with stator flux prediction based on the stator and rotor currents. To regulate the amplitude of the stator voltage, a magnetizing current control is used. Detailed diagram of the scheme is given in Fig. 4 [12–16].

The machine equations written in a synchronously rotating reference frame are given as Eq. (11) [12]:

$$\begin{aligned}
\lambda_{ds} &= L_s i_{ds} + L_m i_{dr} = L_m i_{ms}\\
\lambda_{qs} &= L_s i_{qs} + L_m i_{qr}\\
\lambda_{dr} &= L_m i_{ds} + L_r i_{dr}\\
\lambda_{qr} &= L_m i_{qs} + L_r i_{qr}\\
v_{ds} &= R_s i_{ds} + \frac{d\lambda_{ds}}{dt} - \omega_e \lambda_{qs}\\
v_{qs} &= R_s i_{qs} + \frac{d\lambda_{qs}}{dt} + \omega_e \lambda_{qs}\\
v_{dr} &= R_r i_{dr} + \frac{d\lambda_{dr}}{dt} - (\omega_e - \omega_r)\lambda_{qr}\\
v_{qr} &= R_r i_{qr} + \frac{d\lambda_{qr}}{dt} + (\omega_e - \omega_r)\lambda_{qr}\\
T_e &= 3\frac{p}{2} L_m (i_{qs} i_{dr} - i_{ds} i_{qr})
\end{aligned} \tag{11}$$

where suffix 's' is used for the stator quantities and suffix 'r' is used for the rotor quantities. Similarly suffix 'd' is used for the direct (d)-axis quantities and suffix 'r' is used for the quadrature (q)-axis quantities and all the symbols, used here, have their usual meanings. The equivalent stator magnetizing current is supplied entirely from the rotor side converter. Aligning the d-axis of the reference frame on the stator flux vector gives Eq. (12)

$$i_{qr} = -\frac{L_s}{L_m} i_{qs} \tag{12}$$

Eliminating i_{ds} using the definition for i_{ms} given in (11) and eliminating i_{qs} using the above yields, with $\lambda_{qs}=0$

$$\begin{aligned}
\tau_{ms}\frac{di_{ms}}{dt} + i_{ms} &= i_{dr} + \frac{1+\sigma_s}{R_s} v_{ds}\\
T_e &= -3\frac{p}{2}\frac{L_m^2}{L_s} i_{ms} i_{qr}
\end{aligned} \tag{13}$$

where $\tau_{ms} = L_s/R_s$. Since the last two terms in (13) are zero for constant flux operation, v_{ds} is seen to be small, and also from (13)

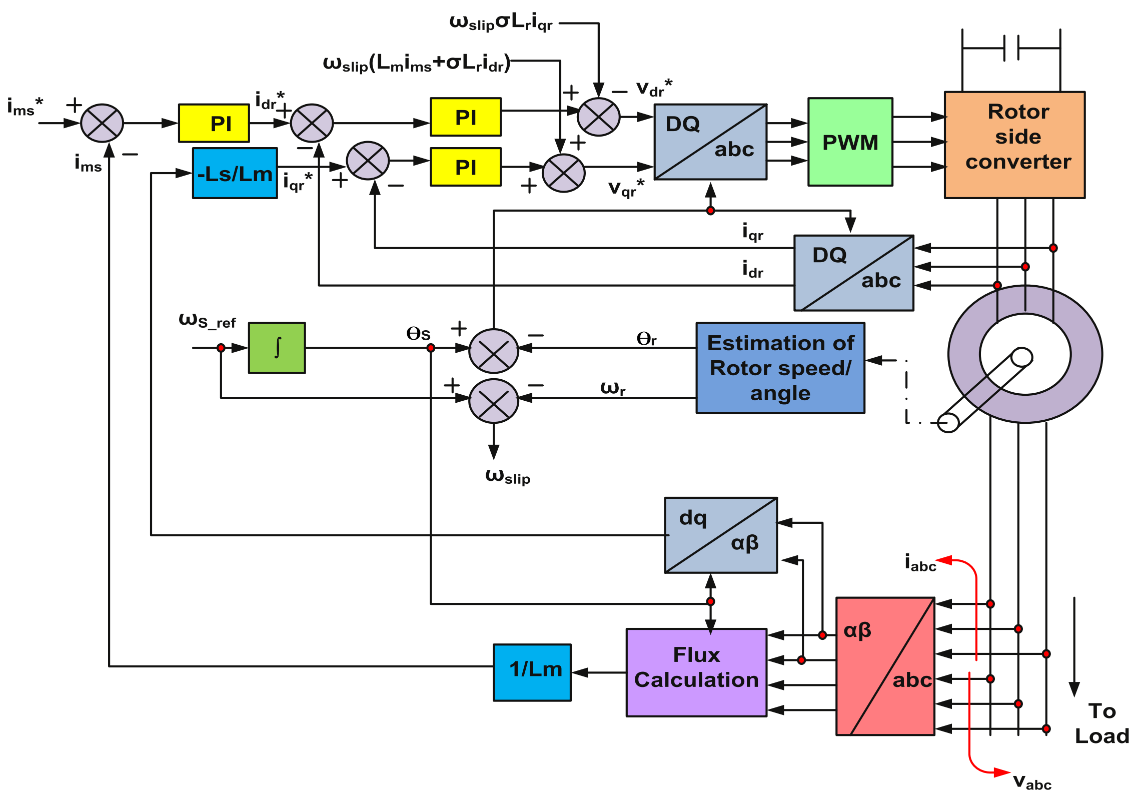


Fig. 4. Block diagram of indirect voltage and frequency control scheme.

it is thus seen that i_{ms} can be controlled using i_{dr}. The rotor current can be controlled according to

$$i^*_{qr} = -\frac{L_s}{L_m} i_{qs} \tag{14}$$

This forces the orientation of the reference frame along the stator flux vector position. The demodulation of the rotor demand voltages uses the slip angle derived from

$$\theta_{slip} = \theta_e - \hat{\theta}_r = \int \omega^*_e \, dt - \hat{\theta}_r \tag{15}$$

where $\hat{\theta}_r$ is the estimated rotor angle (via MRAS observer or open loop observer or speed encoder etc.). The stator flux angle is derived from a free-running integral of the stator frequency demand (50 Hz). This has the advantage that the orientation is shielded from measurement noise and stator voltage harmonics, which may be a problem in a standalone application. A sensorless control method for a stand-alone DFIG system has been projected in [13,14]. The voltage and frequency at the stator terminal are achieved by control of the active and reactive power flows via rotor side converter. Via controlled converter at rotor terminals, rotor currents are regulated in amplitude, frequency, and phase by applying suitable rotor voltages from the rotor side converter. The stator flux-oriented field-control is used for decoupling the active and reactive current control loops to achieve fast dynamic response. The d-axis is associated with the stator flux axis, while the q-axis is associated with the stator voltage vector leading the d-axis by 90°. The q-axis current loop manages the torque of the machine by controlling the active power flow, while d-axis controls the machine flux by controlling the reactive power flow. The proposed method also addresses the power quality problem by incorporating the shunt active filtering concept in stator side converter control. It suffers from the problem of undesirable transients in the machine terminal voltage during load change (as seen from results of the paper).

The paper [17] presents a three phase four wire autonomous Wind Energy Conversion System using doubly fed induction generator feeding local loads. For load harmonic elimination, a zigzag type transformer is used between the stator and stator side converter. Stator/load voltage and frequency control is done via stator side converter. The control scheme for the stator side converter is shown in Fig. 5. The frequency of stator is regulated by generating stator flux angle by integrating the reference stator frequency (50 Hz). Θ is used for transformation of stator voltages and the currents from d to q reference frame to abc reference frame for the control of the stator side converter. The reference value for I^*_{ds} is generated from difference of the reference voltage (V^*_t) and the measured voltage (V_t). The V_t is calculated as

$$V_t = \{(v^2_{ab} + v^2_{bc} + v^2_{ca})/3\}^{1/2} \tag{16}$$

where the v_{ab}, v_{bc} and v_{ca} are instantaneous line voltages at stator side. V^*_t, reference voltage is compared with V_t and error is processed through the PI controller. The output signal of controller gives the I^*_{ds}.

2.2. Direct voltage control (DVC) technique

The DVC [18–32] method is based on stator voltage vector represented in a rotating polar coordinate system by voltage element V and its location regarding angle θ i.e. (V, θ). The reference coordinate system rotates with reference synchronous speed ω^*_s that gives the reference frequency of the generated stator voltage. The control method ensures that the fixed stator voltage vector magnitude $|v_s|$ and the position angle θ_s, related to the d axis, provide the constant voltage magnitude, frequency and controlled voltage phase. The rotor current magnitude and the frequency are directly given the stator voltage PI controllers. The three phase sinusoidal voltage sus,ub, w, are represented in the rotating reference frame d,jq as a vector $\boldsymbol{V}_s$:

$$V_s = v_{sdp} + jv_{sqp} \tag{17}$$

Until the amplitude and frequency of the three phase sinusoidal stator voltage are constant, the stator voltage vector components in (d, jq) coordinates $(v_{sd}v_{sq})$ are constant too, which gives constant value of the voltage vector magnitude $|v_s|$ and position angle θ_s, referred to the d axis of the rotating coordinate system (d, jq). In the DVC method, the components $(v_{sd}v_{sq})$ of the stator voltage vector $\boldsymbol{V}_s$ is used to determine the voltage vector amplitude $|v_s|$ and angle θ_s, as

$$\left|V_s\right| = \sqrt{v^2_{sd} + v^2_{sq}}$$
$$\theta_s = a\ \tan\left(\frac{v_{sq}}{v_{sd}}\right) \tag{18}$$

The stator voltage vector components in (d, jq) coordinate are calculated on the basis of the equations given below

$$v_{sd} = \frac{2}{3}\left(v_{sa}\ \cos(\omega^*_s t) + v_{sb}\ \cos\left(\omega^*_s t - \frac{2}{3}\pi\right) + v_{sc}\ \cos\left(\omega^*_s t + \frac{2}{3}\pi\right)\right)$$
$$v_{sq} = \frac{2}{3}\left(v_{sa}\ \sin(\omega^*_s t) + v_{sb}\ \sin\left(\omega^*_s t - \frac{2}{3}\pi\right) + v_{sc}\ \sin\left(\omega^*_s t + \frac{2}{3}\pi\right)\right) \tag{19}$$

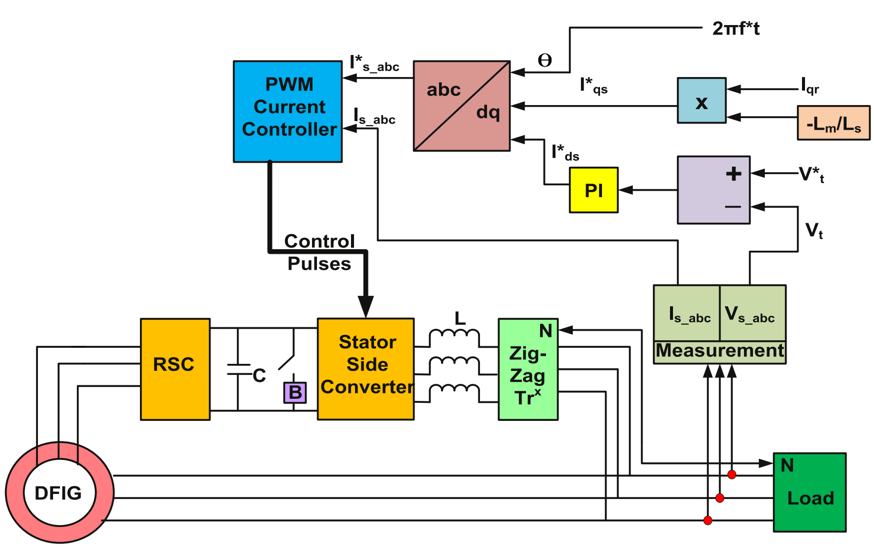


Fig. 5. Voltage and frequency regulation using stator side converter.

Two PI controllers are used in the method. The first PI controller is voltage regulator based on reference $|v_s|^*$ and actual $|v_s|$ stator voltage vector amplitude gives the reference rotor current vector amplitude $|i_r|^*$, and the second one is frequency regulator based on reference θ_s^* and the actual θ_s stator voltage position angle, produces the reference rotor current angular speed

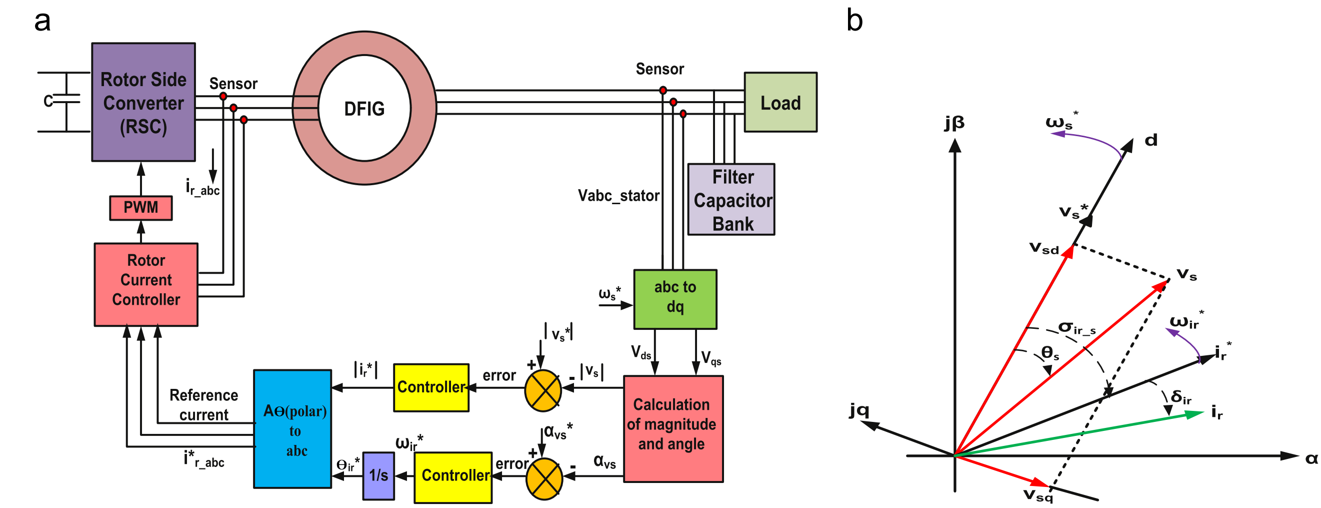


Fig. 6. Direct voltage control method.

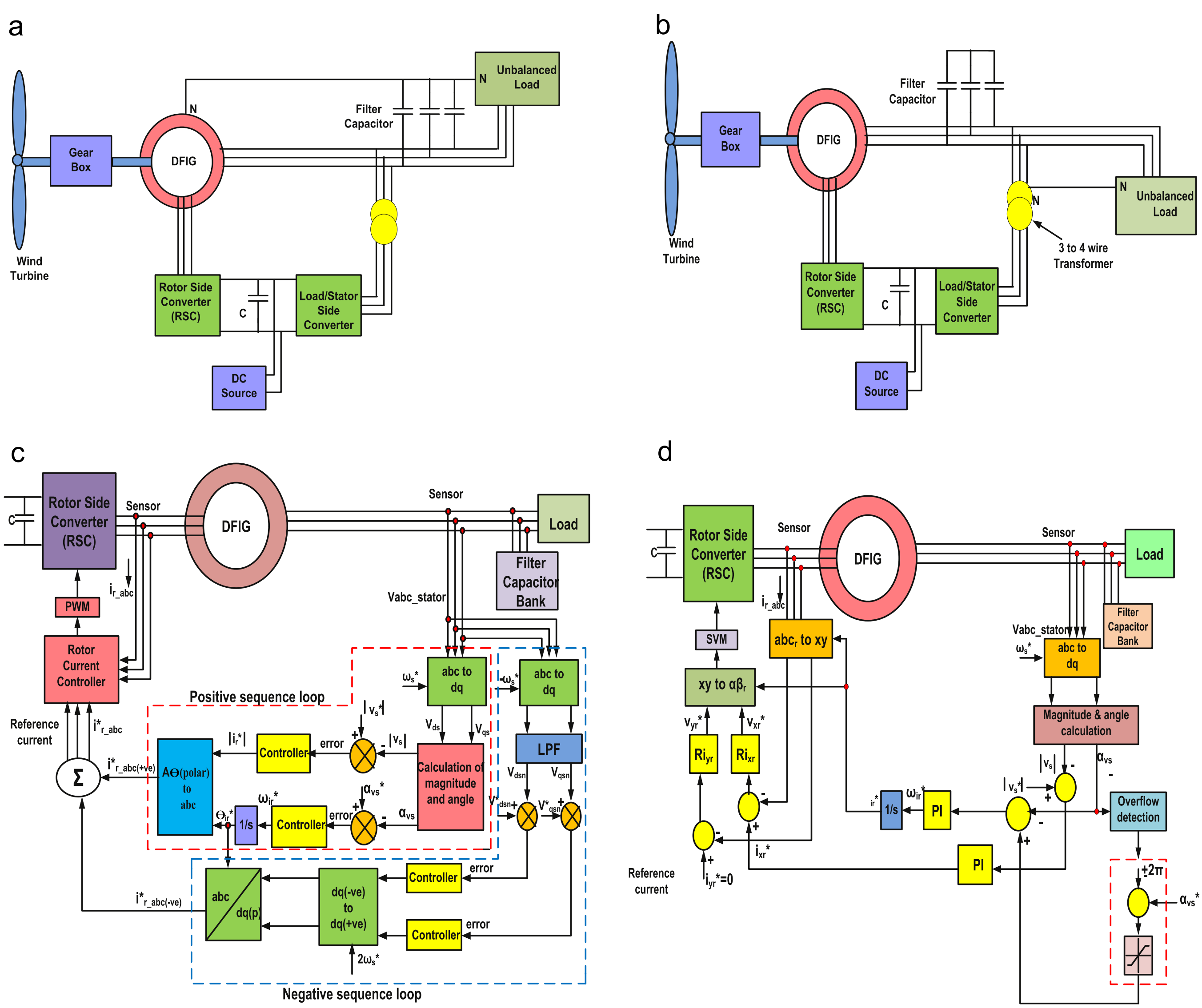


Fig. 7. The load asymmetry/unbalance correction scheme (a) using Neutral wire and (b) using 3 to 4 wire transformer.

$|\omega_{ir}|^*$. After the integration of output signal $|\omega_{ir}|^*$ of frequency regulator gives the reference rotor current vector position angle θ_{ir}^* with respect to rotor (Fig. 6a).

The conversion from polar (A, θ) coordinates to Cartesian $(a\ b\ c)$ coordinates referred to the rotor provides the three phase reference rotor current signals i_{ra}^*, i_{rb}^*, i_{rc}^* for rotor current

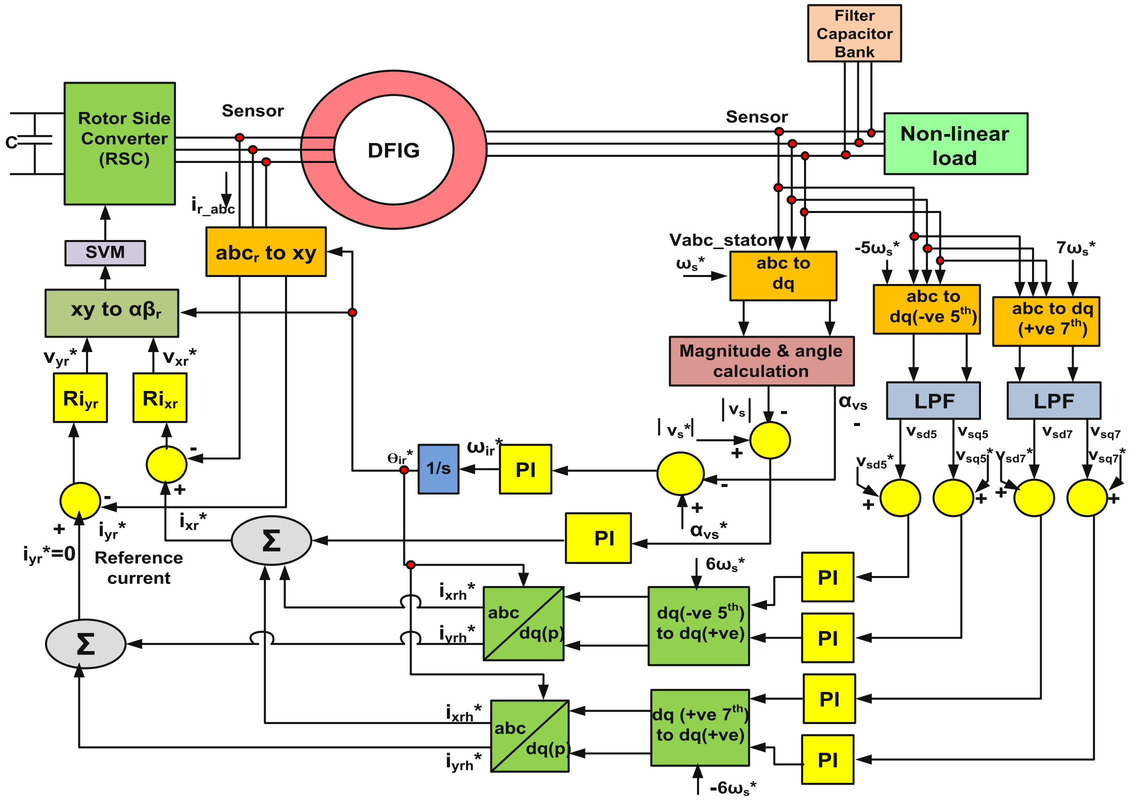


Fig. 8. Load harmonics (5th and 7th) mitigation scheme.

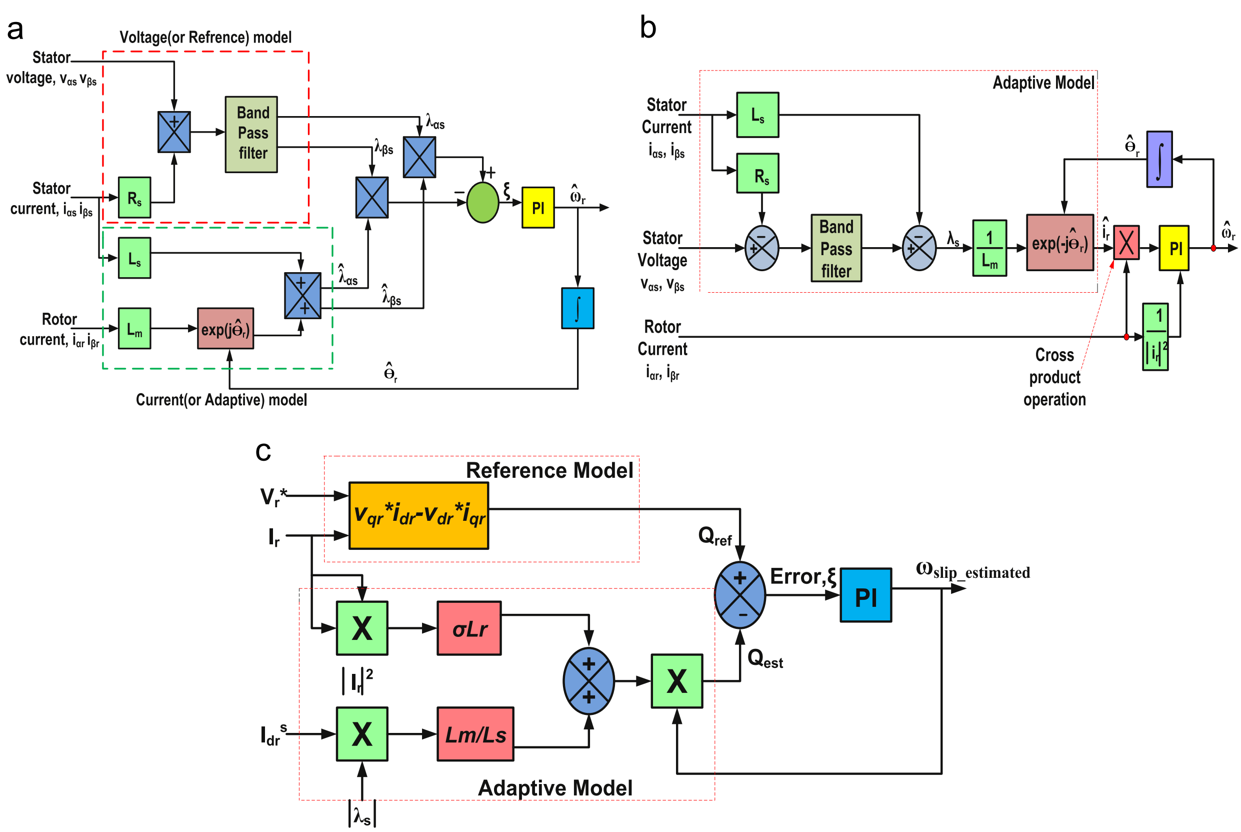


Fig. 9. (a) Stator-flux-based MRAS observer (SFMO); (b) rotor current based MRAS observer (RCMO); (c) reactive power based MRAS Observer (Q-MRAS).

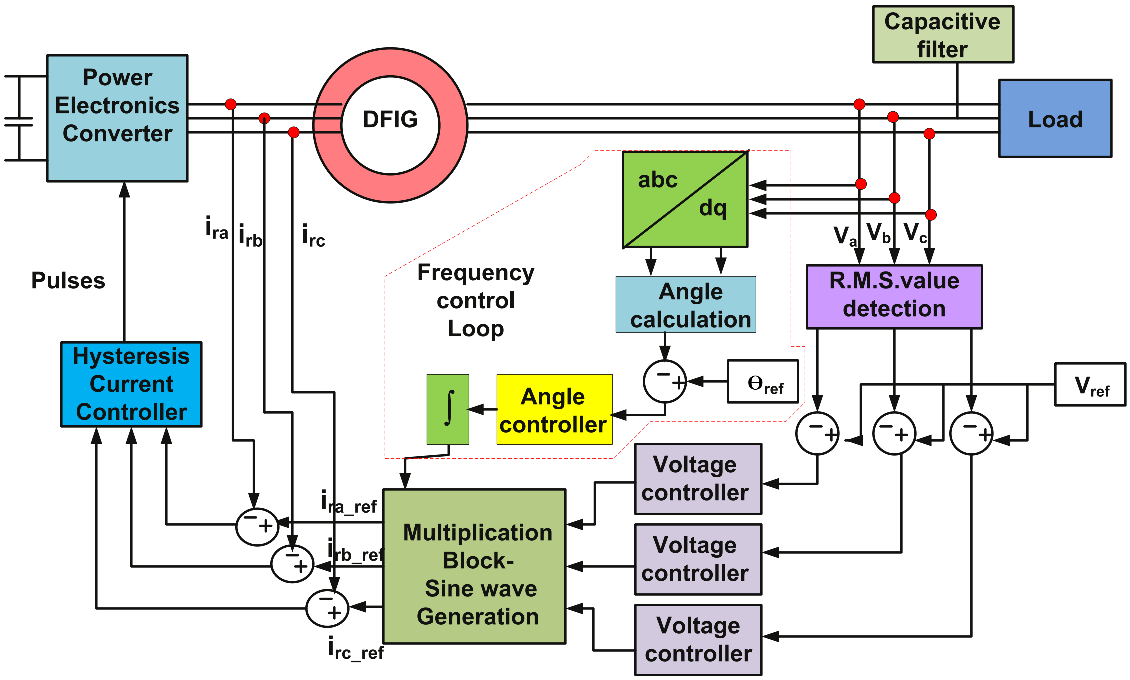


Fig. 10. Proposed control technique.

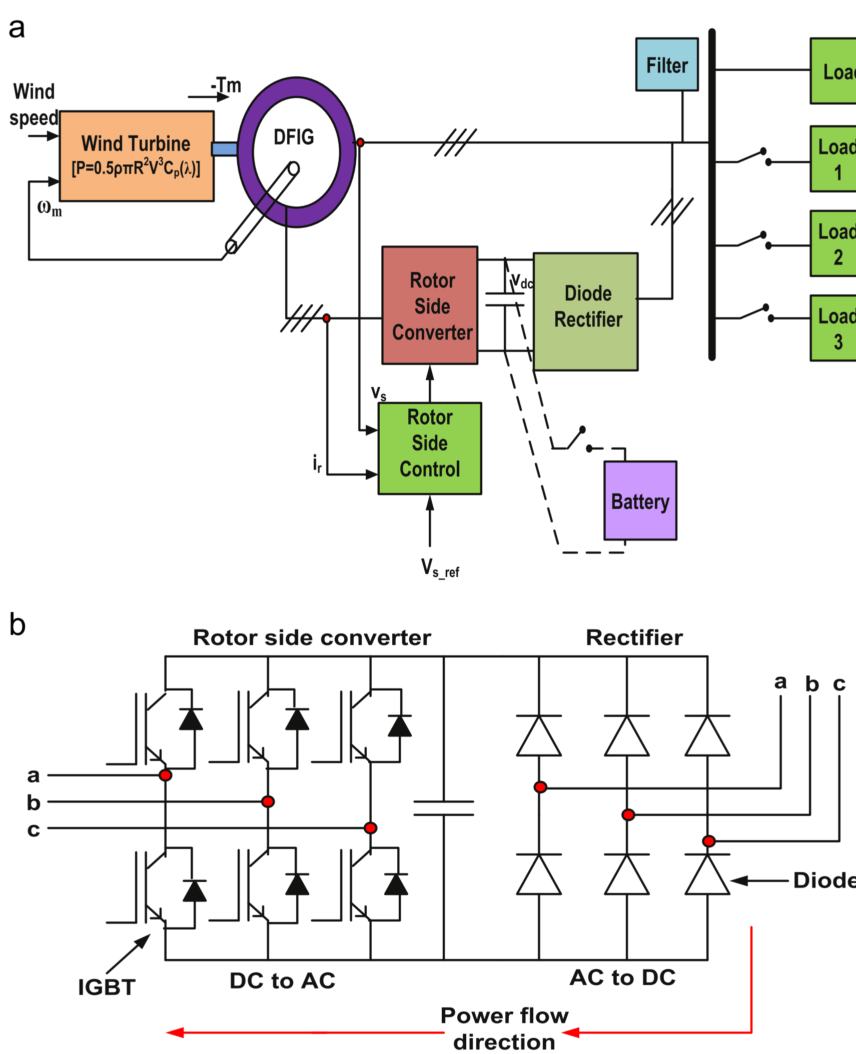


Fig. 11. (a) Simulation block diagrams of system and (b) detailed diagram dc-link converter.

Table 1
Data specification table.

S.N.	DFIG parameter	Value
1.	Nominal rated power	2 MVA
2.	Rated line-to-line stator voltage (V_{rms})	690 V
3.	Rated line-to-line rotor voltage (V_{rms})	2070 V
4.	Stator and rotor connection	Star and star
5.	Nominal frequency	50 Hz
6.	Stator resistance and leakage inductance	2.6 mΩ and 0.087 mH
7.	Rotor resistance and leakage inductance	26.1 mΩ and 0.783 mH
8	Magnetization inductance	2.5 mH
9.	No. of pole pair	2
10.	Matching transformer rating	1 MVA, 690/2070V_{rms}
11.	Sampling time	10 μs
	Power electronics converter data	**Value**
12.	IGBT switch (6 no.)	3300 V, 1200 A
13.	Power diode (6 no.)	2000V_{rms}, 1000 A

controllers.

$$\begin{bmatrix} i_{ra}^* \\ i_{rb}^* \\ i_{rc}^* \end{bmatrix} = |i_r|^* \cos \begin{bmatrix} \theta_{ir}^* \\ \theta_{ir}^* - 2\pi/3 \\ \theta_{ir}^* + 2\pi/3 \end{bmatrix} \tag{20}$$

The reference voltage vector $|v_s|^*$ is coincided with the d axis of the reference coordinate system in the steady state. In the transient state, the actual stator voltage vector $|v_s|$ is displaced from the reference position $|v_s|^*$ by the angle θ_s, because the actual rotor current vector i_r is displaced from its reference position i_r^* by angle δ_{ir} (Fig. 6b). On basis of the actual position angle θ_s of the stator voltage vector $\boldsymbol{V}_s$, the frequency regulator regulates the rotor current angular speed $|\omega_{ir}|^*$ concerning the rotor current vector acceleration or deceleration. It makes certain that the rotor current vector position angle is changed and the vector achieves its reference position i_r^* and accordingly the reference position of the stator voltage is achieved and the θ_s displacement angle is omitted (Fig. 6b).

Due to unbalanced load, the voltages at point of common coupling (PCC) become unbalanced. Unbalanced load will create pulsation in the generator torque which will reduce the life of the turbine shaft. In the case of DFIG based stand-alone WEGSs, even few percent of the load asymmetry causes the output voltage strongly unbalanced. In [25–30], authors give solution for the load asymmetry/unbalance. For the small percentage of load asymmetry a star connected stator with the neutral wire or three to four wire matching transformer is used, Fig. 7(a) and (b). For the larger unbalance in load, extended direct voltage control based on positive and negative sequence components was given. The method uses positively rotated polar frame for the control magnitude and frequency of stator voltage and the negative sequence components for load asymmetry/unbalance correction are used (Fig. 7(c) and (d)).

An improvement in the DVC method for the non-linear load is presented in [31]. The relatively large stator side filtering capacitors C_f provide significant decrease in higher harmonics including switching frequency harmonics. But the C_f is increased within limits only (as discussed in Section 2) it must not fully compensate the magnetizing reactive power of machine. Stator voltage harmonics caused by nonlinear load can be removed by PI regulators implemented for each harmonics in the coordinate system rotated with the speed corresponded to respective harmonics. Typically, the three phase nonlinear load induces mainly negative sequence 5th harmonics, positive sequence 7th harmonics and considerably smaller amount of higher harmonics. Noticeably relatively large stator side filtering capacitors C_f, provide significant reduction of higher harmonics including switching frequency harmonics. The 5th and 7th harmonics control parts are presented in Fig. 8. Three phase stator voltage v_{abc_stator} is converted into the negatively rotated $(-5\omega_s^*)$ coordinated system associated with 5th harmonic and into the positively rotated $(-7\omega_s^*)$ coordinated system associated with 7th harmonic. To obtain dc components representing the dq coordinated system, low pass filters with 20 Hz of cut-off frequency are used.

A direct voltage control is implemented in [32] via hysteresis current control. The performance study of DFIG was observed, when it supplies the isolated (R–L type) load, in MatLab/simulink only.

2.3. MRAS observer based control technique

The Model Reference Adaptive System (MRAS) observers are the recognized method for the sensorless control of cage induction machines [33,34], there are a small number of information related to the application of MRAS observers for sensorless control of autonomous DFIG systems. It is well known that the use of open loop kind of observers might present significant estimation errors when model uncertainties are present. Then, the use of a closed loop observer is a good choice to improve the steady state and transient behavior of the control system. A MRAS speed observer is used to estimate the rotational speed and rotor position of the DFIM. In the literature, there are five basic types of MRAS observers; stator-flux-based MRAS observer (SFMO); stator current based MRAS observer (SCMO); rotor current based MRAS observer (RCMO); rotor flux based MRAS observer (RFMO); Reactive power based MRAS observer (Q-MRAS). In [3], a rotor-flux-based sensorless scheme is reported, where the rotor flux is obtained by the integration of the rotor back-electromotive force. This approach suffers from integration problems, with poor performance when the machine operates about synchronous speed, because the rotor is excited with low frequency voltages.

The stator flux based observer [35–38,50–54] is derived from two models; the voltage model and the current model.

In a stationary frame, the voltage model is used to obtain the stator flux as

$$\lambda_s = \int (v_s - R_s i_s)\, dt \tag{21}$$

The stator voltage drop R_s will be small under rated operation so that the flux estimate of (15) is relatively insensitive to R_s. Using a stationary frame, the stator flux is obtained from the current model as

$$\widehat{\lambda}_s = L_s i_s + L_m i_r e^{j\widehat{\omega}_r t} \tag{22}$$

where $\widehat{\omega}_r$ is an estimation of the rotational speed.

The current is referred to the rotor frame. In the MRAS observer, the flux obtained from the voltage model is used as the reference flux. By adjusting the estimated rotational speed, the error between the reference flux and the flux estimated from current model is reduced. The error in (α, β) coordinates is defined as

$$\xi = \hat{\lambda}_{\alpha s}\lambda_{\beta s} - \lambda_{\alpha s}\hat{\lambda}_{\beta s} \tag{23}$$

The error (given above) is driven to zero by means of a proportional-integral (PI) controller. The output of this PI controller is the estimated rotational speed used. Fig. 9(a) shows a block diagram of the stator flux based MRAS observer.

In [40–45] a rotor-current-based MRAS observer scheme is reported. The observer estimates the rotor speed and position using the rotor current i_r in the rotor frame. This current can be obtained from direct measurements via transducers and transformed to its two-phase equivalent $i_{\alpha r}$, $i_{\beta r}$. This is the reference

model for the MRAS observer. This current is compared with an estimated rotor current obtained from the stator voltage v_s and current i_s referred to the rotor frame using an estimation of the rotor position $\hat{\theta}_r$. This is the adaptive model for the MRAS observer. The estimated rotor $\hat{i}_r$ is obtained as

$$\lambda_s = L_s i_s + L_m i_r e^{j\theta_r t} = \int (v_s - R_s i_s)\, dt$$
$$\hat{i}_r = \frac{1}{L_m}(\lambda_s - L_s i_s)e^{-j\hat{\theta}_r t} \tag{24}$$

The error between the measured rotor current and the estimated from (24) can be expressed as

$$\xi = \hat{i}_{\alpha r} i_{\beta r} - i_{\alpha r}\hat{i}_{\beta r} \tag{25}$$

where $i_{\alpha r}$, $i_{\beta r}$, $\hat{i}_{\alpha r}$, $\hat{i}_{\beta r}$ are the measured and estimated rotor currents in α–β stationary reference frame affixed to the rotor. The error in (25) is the cross product between the real and estimated rotor current vectors. This cross product can be calculated as

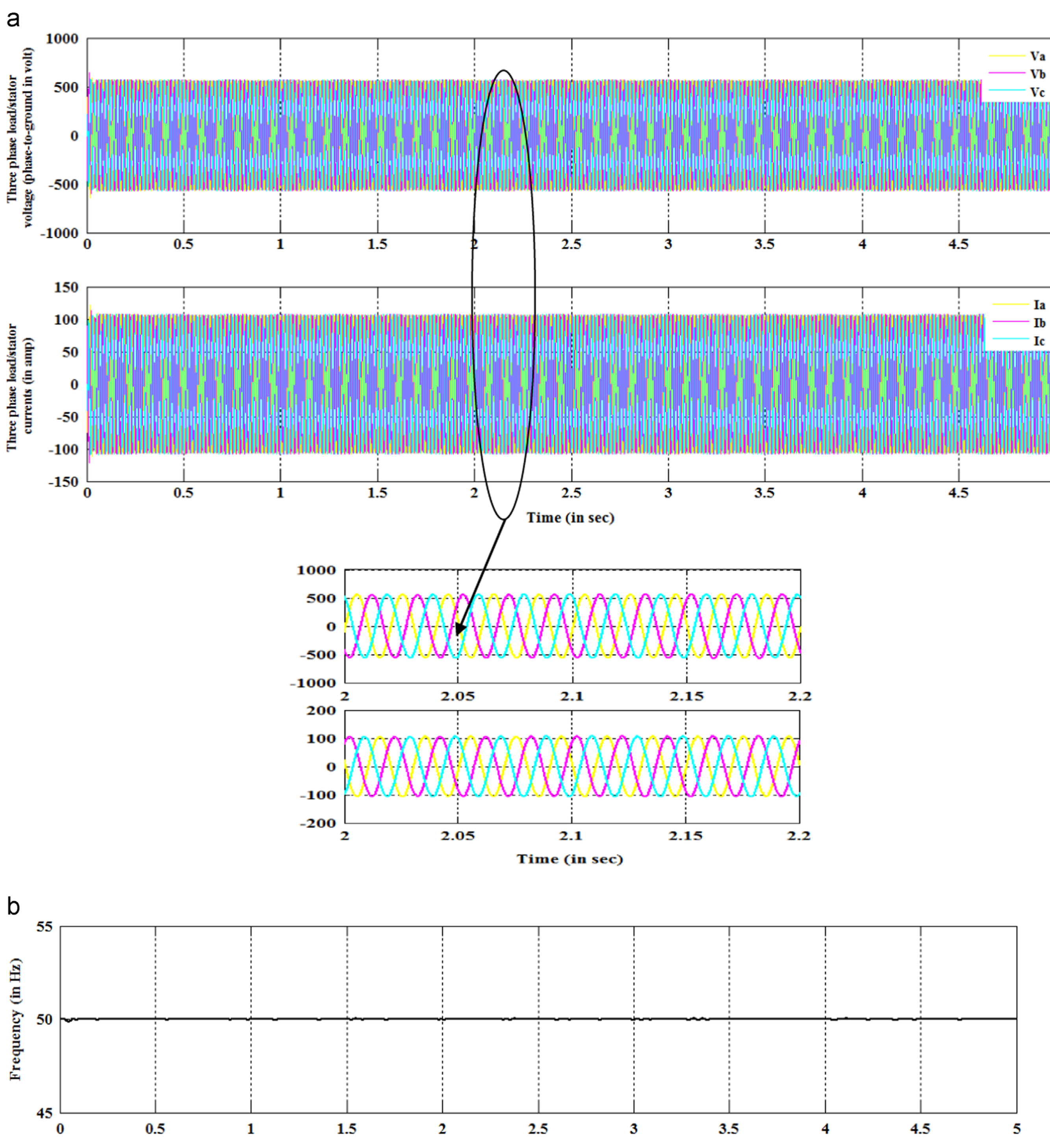


Fig. 12. (a) Load voltage (V_{abc} in volts) and current (I_{abc} in amp) and (b) frequency of stator load/stator voltage.

follows:

$$\xi = \hat{i}_r \times i_r = |\hat{i}_r|\ |i_r|\ \sin(\theta_{error}) \quad (26)$$

where θ_{error} is the angle between the real and estimated rotor current vectors $\hat{i}_r$ and i_r respectively. A PI controller is used to process the error in (26). The output of the controller is the estimated speed. The controller adjusts the estimated speed in order to achieve $\theta_{error} = 0$, resulting in a correct estimation of the rotor position and speed. Fig. 9(b) shows a block diagram of the MRAS observer.

The fundamental model of the reactive power based MRAS observer (Q-MRAS) [46,47] consists of the reference model, computes the instantaneous rotor side reactive power (Q_{ref}) according to (29) and the adaptive model gives the steady state reactive power (Q_{est}) using (31). The implementation of the Q-MRAS is shown in Fig. 9(c).

In the stator flux oriented reference frame, the rotor voltage equations are given as [47]

$$v^*_{dr} = R_r i^s_{dr} - \omega_{slip}\lambda^s_{qr} + \frac{d}{dt}\lambda^s_{dr} \quad (27)$$

$$v^*_{qr} = R_r i^s_{qr} + \omega_{slip}\lambda^s_{dr} + \frac{d}{dt}\lambda^s_{qr} \quad (28)$$

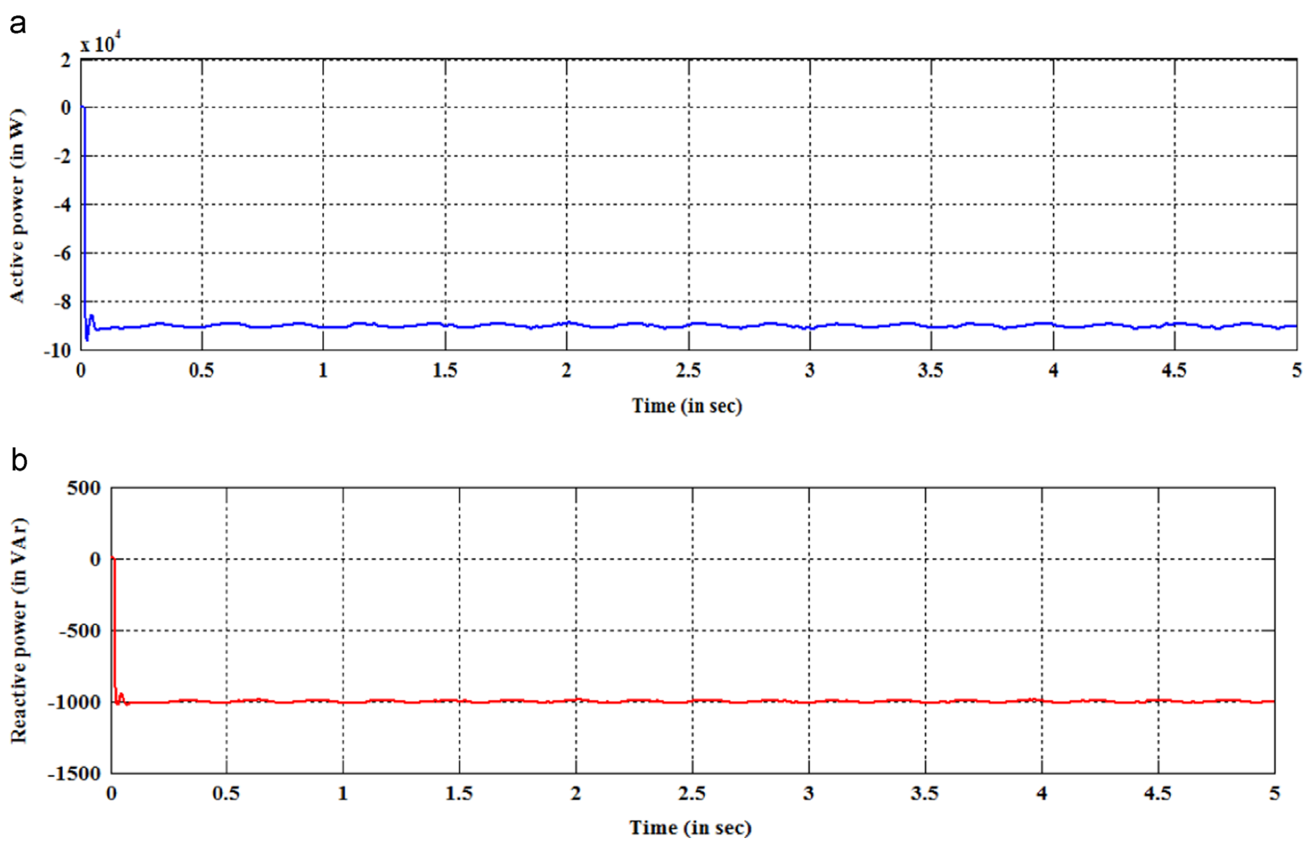


Fig. 13. (a) Active power (in W) and (b) reactive power (in W).

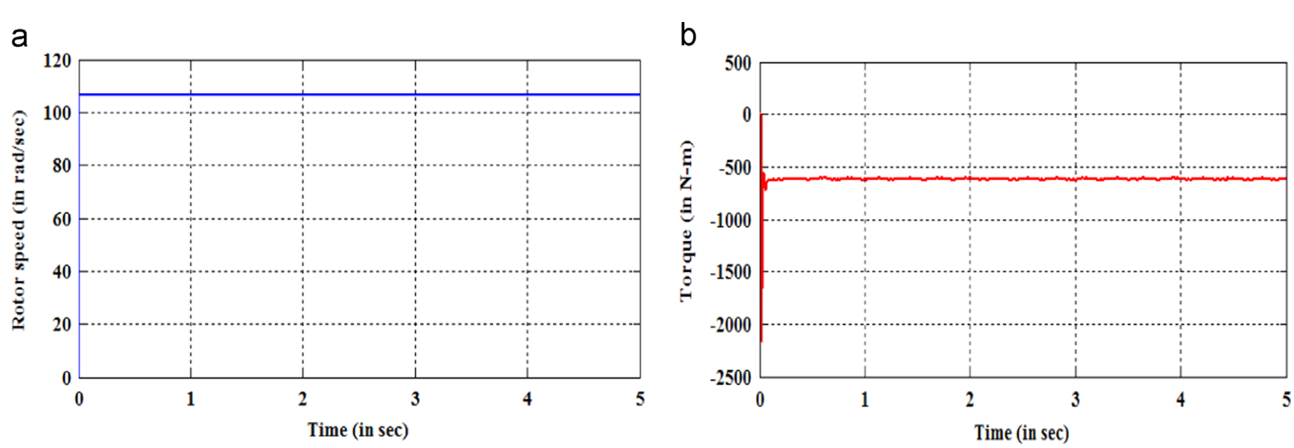


Fig. 14. (a) Generator speed (in rad/s) and (b) torque (in N m).

The instantaneous reactive power is given as

$$Q_{ref} = V_r \otimes I_r = v_{qr} i_{dr} - v_{dr} i_{qr} \quad (29)$$

For the reference Q^*_{ref}

$$Q^*_{ref} \approx v^*_{qr} i_{dr} - v^*_{dr} i_{qr} \quad (30)$$

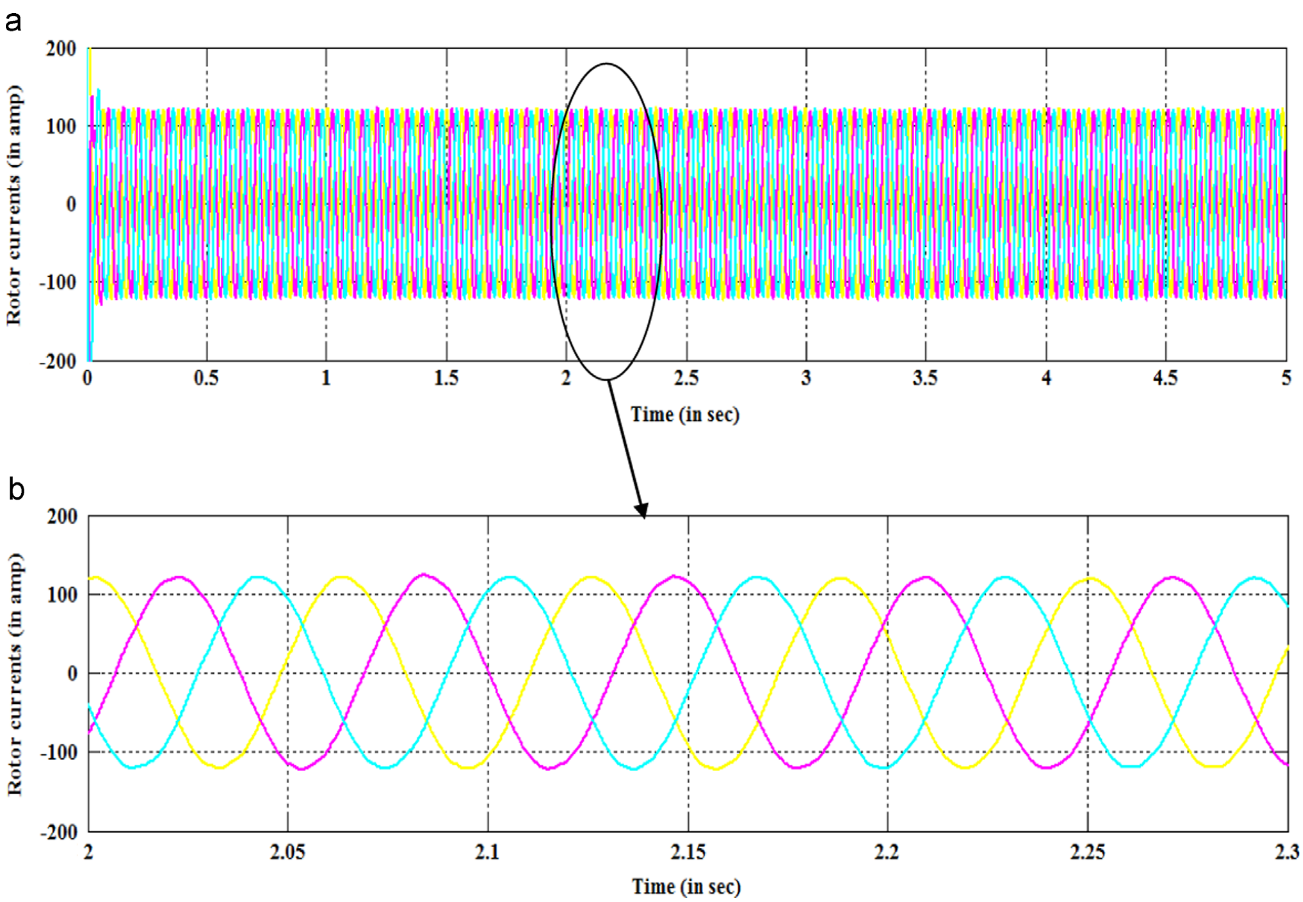


Fig. 15. (a) Rotor current (in amp).

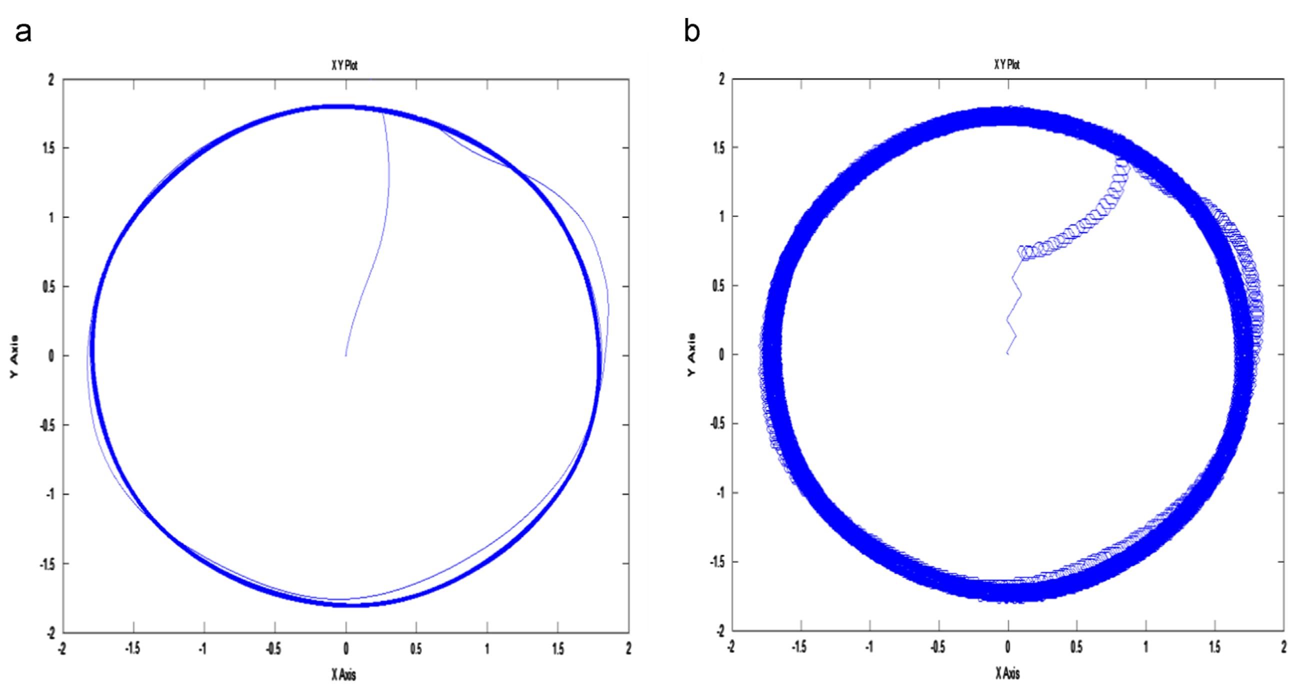


Fig. 16. (a) Rotor flux in d–q plan and (b) stator flux in d–q plan.

Substituting (27) and (28) into (30), and under the stator flux orientation, the expression of Q_{est} at steady state becomes

$$Q_{est} = \omega_{slip_estimated}\left[\sigma I_r I_r^2 + \frac{L_m}{L_s}\lambda_s i_{dr}^s\right] \quad (31)$$

Q_{est} is free from the variation of the rotor resistance. The MRAS observer error is given by

$$\xi = Q_{ref} - Q_{est} \quad (32)$$

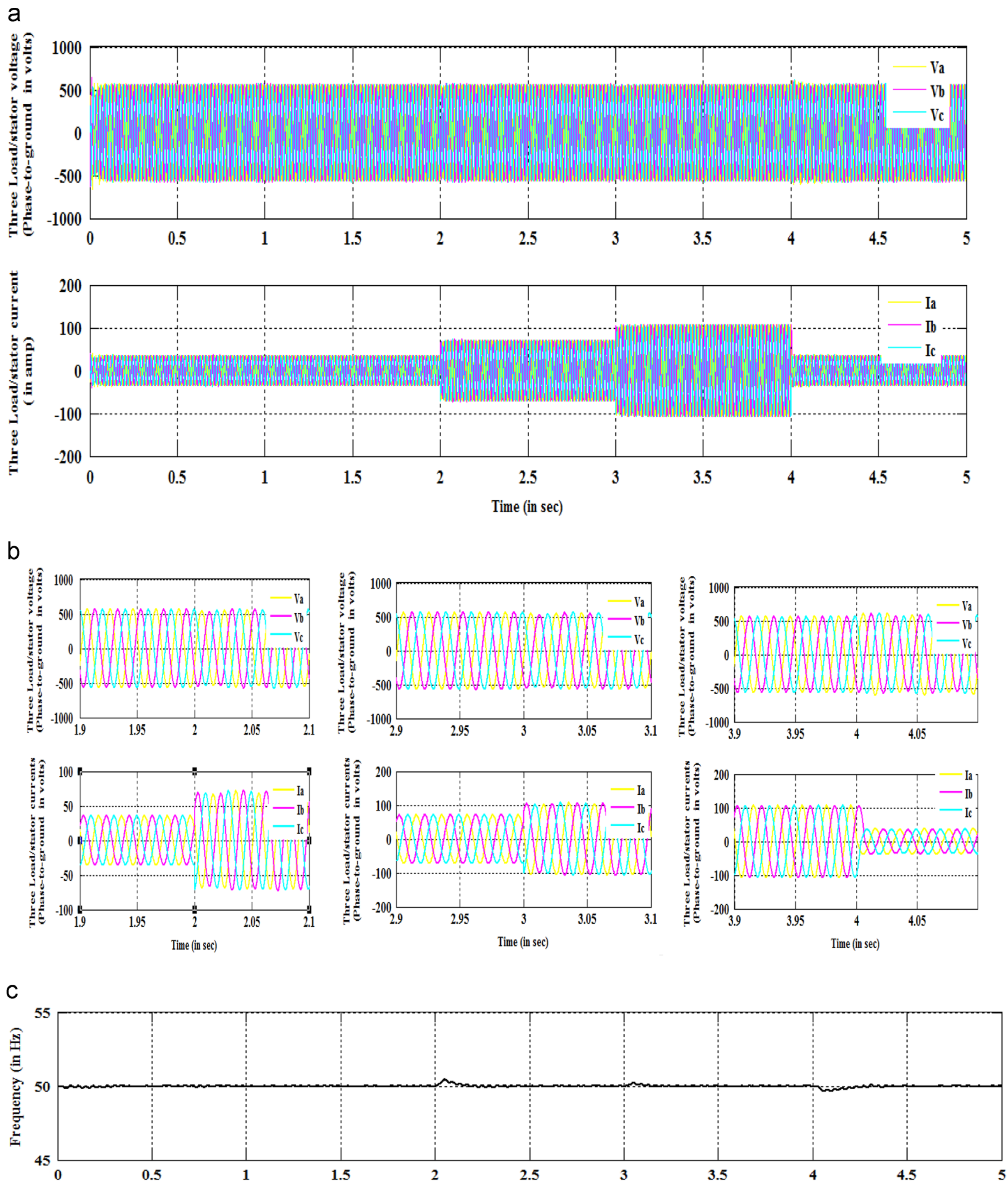


Fig. 17. (a) Load voltage (V_{abc} in volts) and current (I_{abc} in amp); (b) enlarged views of (a); (c) frequency of load/stator voltage.

The error (ε) is processed through a PI controller and output signal is the estimated slip speed ($\omega_{slip_estimated}$). This estimated slip speed ($\omega_{slip_estimated}$) is used to tune the adaptive model such that error (ξ) tends to zero.

The comparative performance of stator flux based MRAS observer and rotor current based MRAS observers are good for both stand-alone and grid connected systems as show in the paper. But these schemes cannot be used for the rotational speed of an already rotating machine (i.e. "speed catching on the fly"), without the knowledge of any initial condition [46]. For the sensorless stand-alone DFIG WECS, it is desirable to be able to estimate the speed of the rotation of an already rotating machine. However, MRAS speed observers, discussed so far, are not capable of "speed catching on the fly". The Q-MRAS is suitable for speed catching operation. But it gives incorrect results of speed estimation when the direct-component of rotor current and ratio (L_m/L_s) is varied [46,47].

Some latest Refs. [54–59] are available in the literature which addresses the voltage and frequency control in stand-alone DFIG based WECS but there control scheme is associated with speed sensor/encoder.

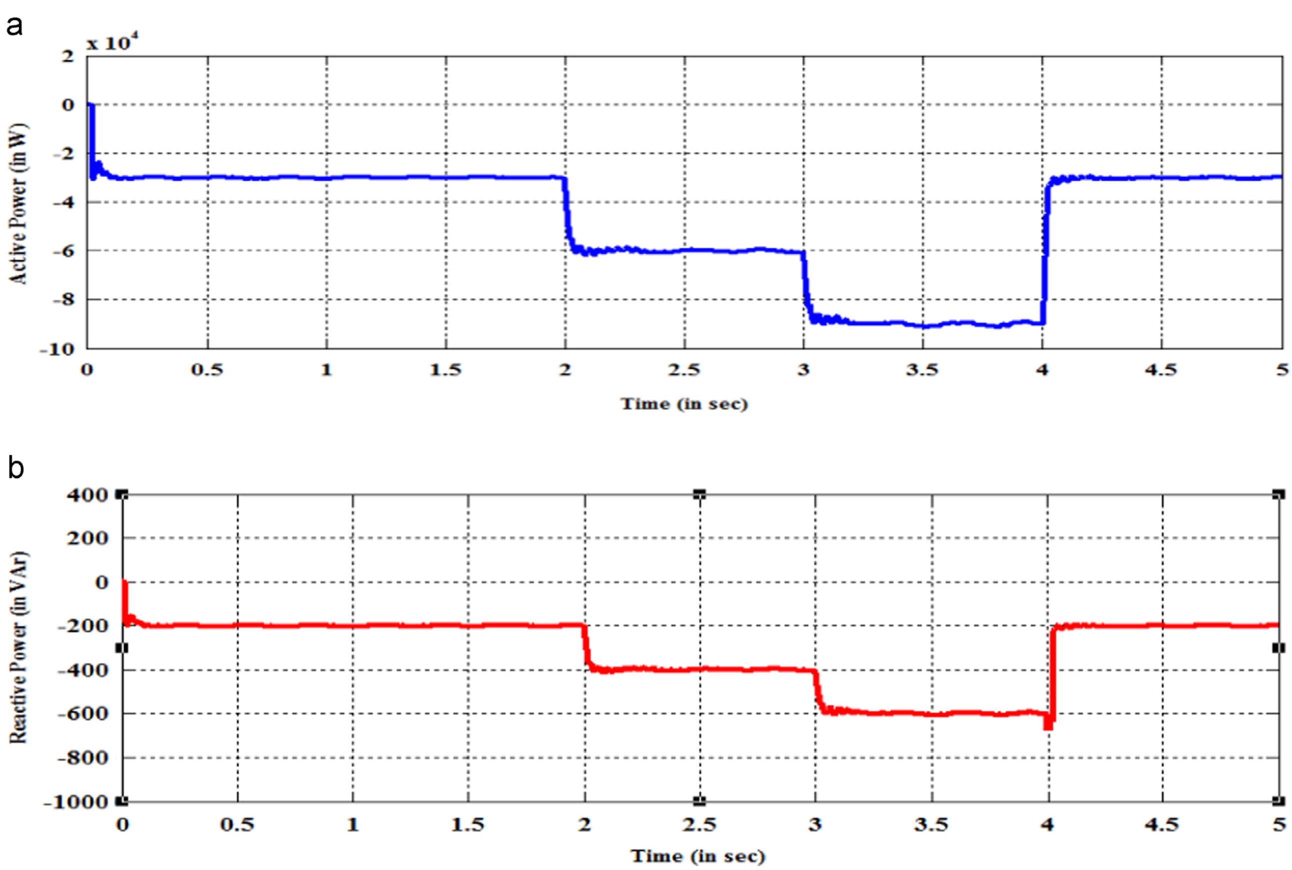


Fig. 18. (a) Active power (in W) and (b) reactive power (in W).

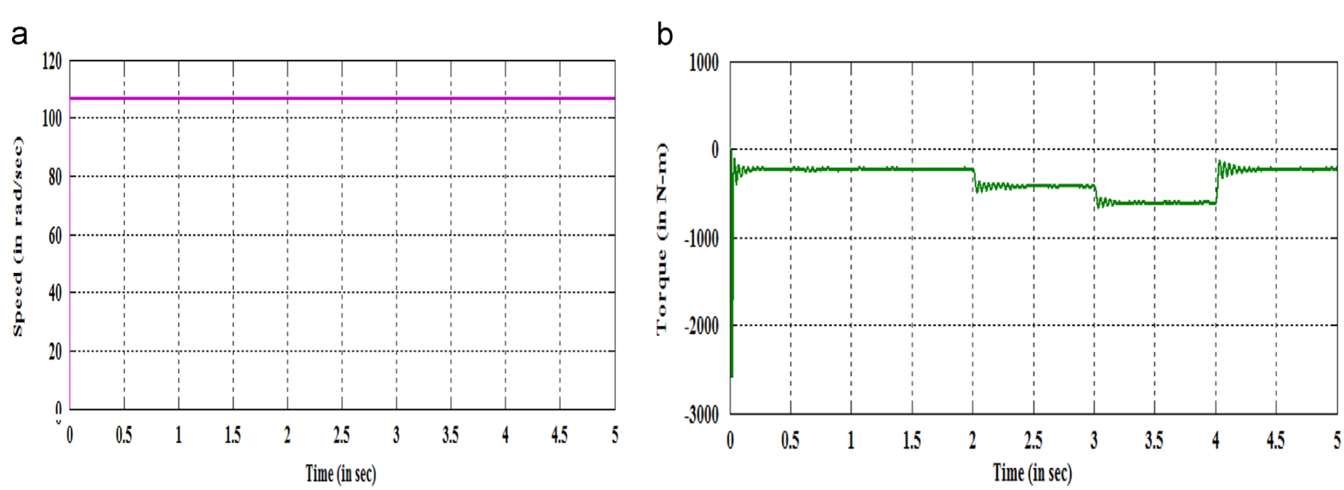


Fig. 19. (a) Generator speed (in rad/s) and (b) torque (in N m).

3. Proposed control technique

Fig. 10 shows a full scheme of stator voltage and frequency control based on the root mean square (rms) detection scheme. The per phase rms value of the stator voltage is detected, the basic principal of the detector [60] is given below in this section. To control the amplitude of the output voltage, the error between the rms value of the phase voltages at point of common coupling (PCC) or output terminal and the reference phase voltage is given to a PI controller. For the frequency control, a PLL based frequency control loop is designed to obtain the desired frequency at output (such as in Direct Voltage Control method). The synchronous (50 Hz or 314 rad/s) reference frame is used for the purpose. A PI controller (called frequency controller) is used to obtain the error measured angle and reference angle (i.e. zero). This error gives the reference speed of the rotor currents after the integration we find the reference frequency of the rotor currents. The reference frequency signal and amplitude controller output are combined in sine wave generator block to obtain the reference phase currents ira_ref, irb_ref and irc_ref. These reference phase currents are compared with measured phase currents and pulses are generated to switch ON/OFF the rotor side power electronics converter via hysteresis controller.

R.M.S. detector: The basic principal of R.M.S detector is as follows:

Assuming that the input voltage $v_s(t)$ is given by

$$v_s(t) = \sqrt{2}V_s \sin(\omega t) \tag{33}$$

Where V_s *is* the rms value of the input voltage. If v_s is passed through a 90° phase shifting circuit, then $v_s'(t)$ is obtained as

$$v_s'(t) = \sqrt{2}V_s \sin(\omega t + 90^\circ) = v_s'(t) = \sqrt{2}V_s \cos(\omega t) \tag{34}$$

The two signals, $v_s(t)$ and $v_s'(t)$, are a pair of orthogonal functions. If they are passed through two separate multipliers and squared, the following two equations can be obtained.

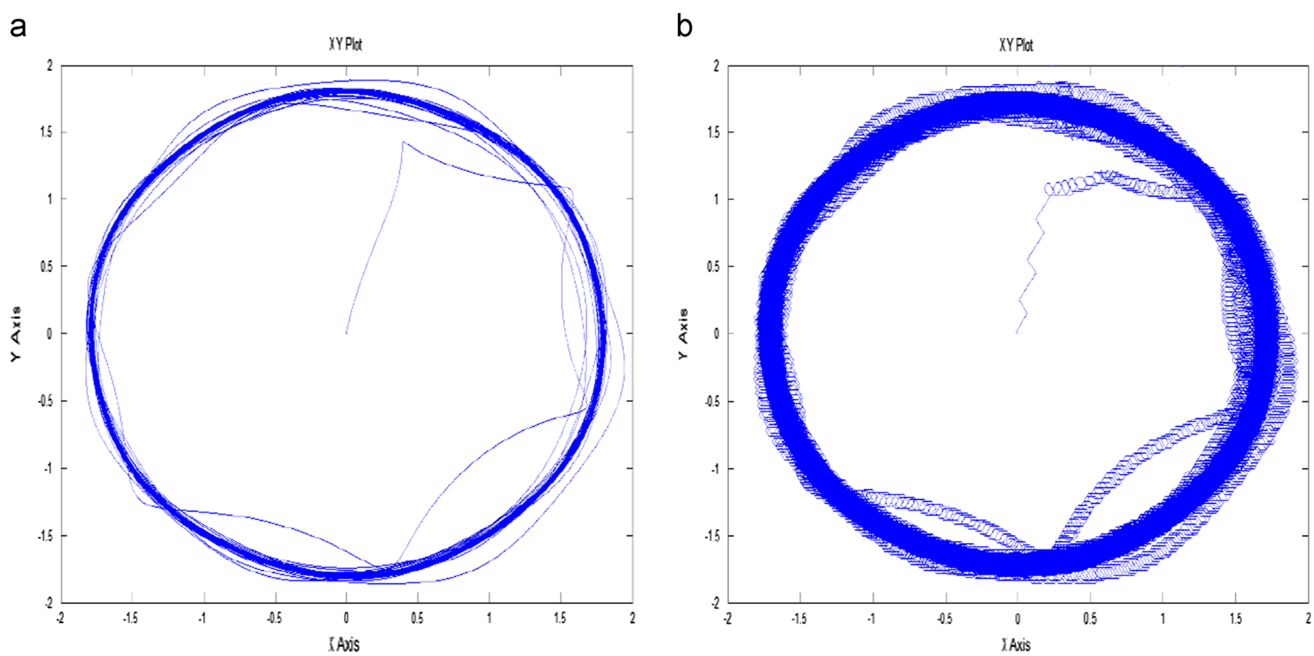


Fig. 20. (a) Rotor flux in d–q plan; (b) stator flux in d–q plan.

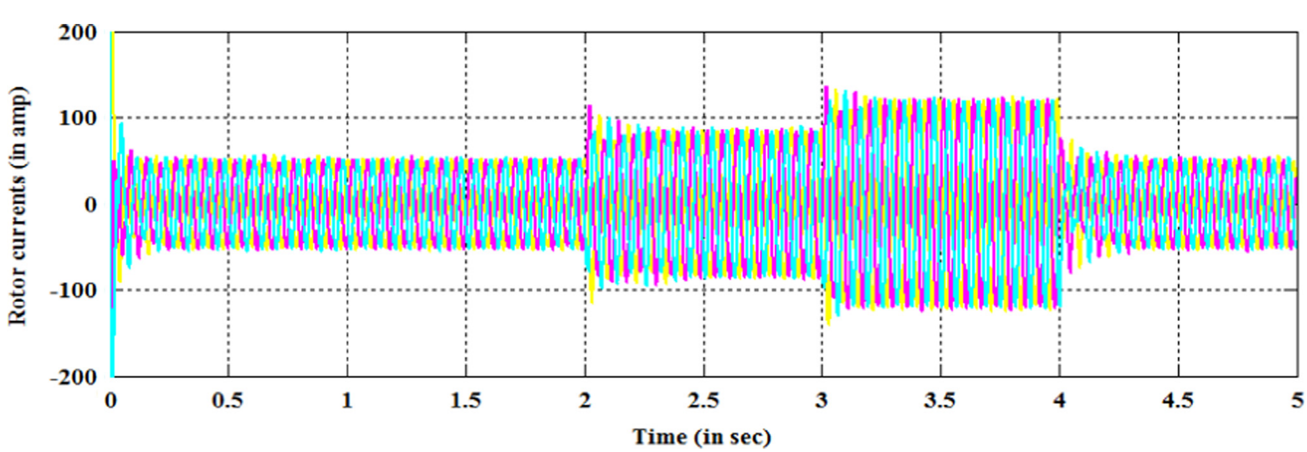


Fig. 21. Rotor current (in amp).

Squaring and adding Eqs. (33) and (34) we get

$$v_{o1}(t) = k2V_s^2 \sin^2(\omega t) \quad (35)$$

$$v_{o2}(t) = k2V_s^2 \cos^2(\omega t) \quad (36)$$

where k is the multiplication factor of the multipliers and it is set to be 0.5. Because of the characteristic of orthogonal functions $v_{o1}(t)$ and $v_{o2}(t)$ we can easily obtain the square of the input voltage rms value by adding (35) and (36):

$$\begin{aligned} v_o(t) &= v_{o1}(t) + v_{o2}(t) \\ &= k2V_s^2 \sin^2(\omega t) + k2V_s^2 \cos^2(\omega t) \\ &= 0.5.2.V_s^2 = V_s^2 \end{aligned}$$

In order to measure the rms value, the signal $v_o(t)$ is fed to a square root circuit.

Sine wave generation:

Here output of controllers is multiplied with unit amplitude sine wave signals whose frequency is decided by the frequency control loop:

$$S_a(t) = A_a \sin(\omega t)$$

$$S_b(t) = A_b \sin\left(\omega t + \frac{2\pi}{3}\right)$$

$$S_c(t) = A_c \sin\left(\omega t + \frac{4\pi}{3}\right)$$

where A_a, A_b and A_c are the output signals of amplitude controllers and ω is decided by the frequency loop.

4. Results and discussion

The simulation model of the DFIG based variable speed wind turbine system (shown in Fig. 11(a)) is built using MATLAB/SIMULINK. The simulation parameters and rating of power electronics converters (shown in Fig. 11(b)) are given in Table 1. In this paper we have taken four cases. Case 1 shows the steady state operation i.e. constant load and constant wind speed operation of the system; case 2 shows the loads switching operation of the system when wind speed is constant; case 3 shows the system performance when wind speed is variable and load is constant; and case 4 shows the unbalanced load operation of the system and wind speed is constant. A battery (as dc source) is connected for time period 0–0.1 s to give 690V_{rms} line-to-line (or 976 V peak), and result shows that generated stator voltage follows the reference value and stays at the specified value (i.e. 976 V peak) and frequency of generated stator voltage is equal to 50 Hz in both the cases.

Case 1: In this case, we show a steady state operation of the system. A load of 90 kW and 1 kVAR is connected throughout the simulation, i.e. 0–5 s. The results are shown below.

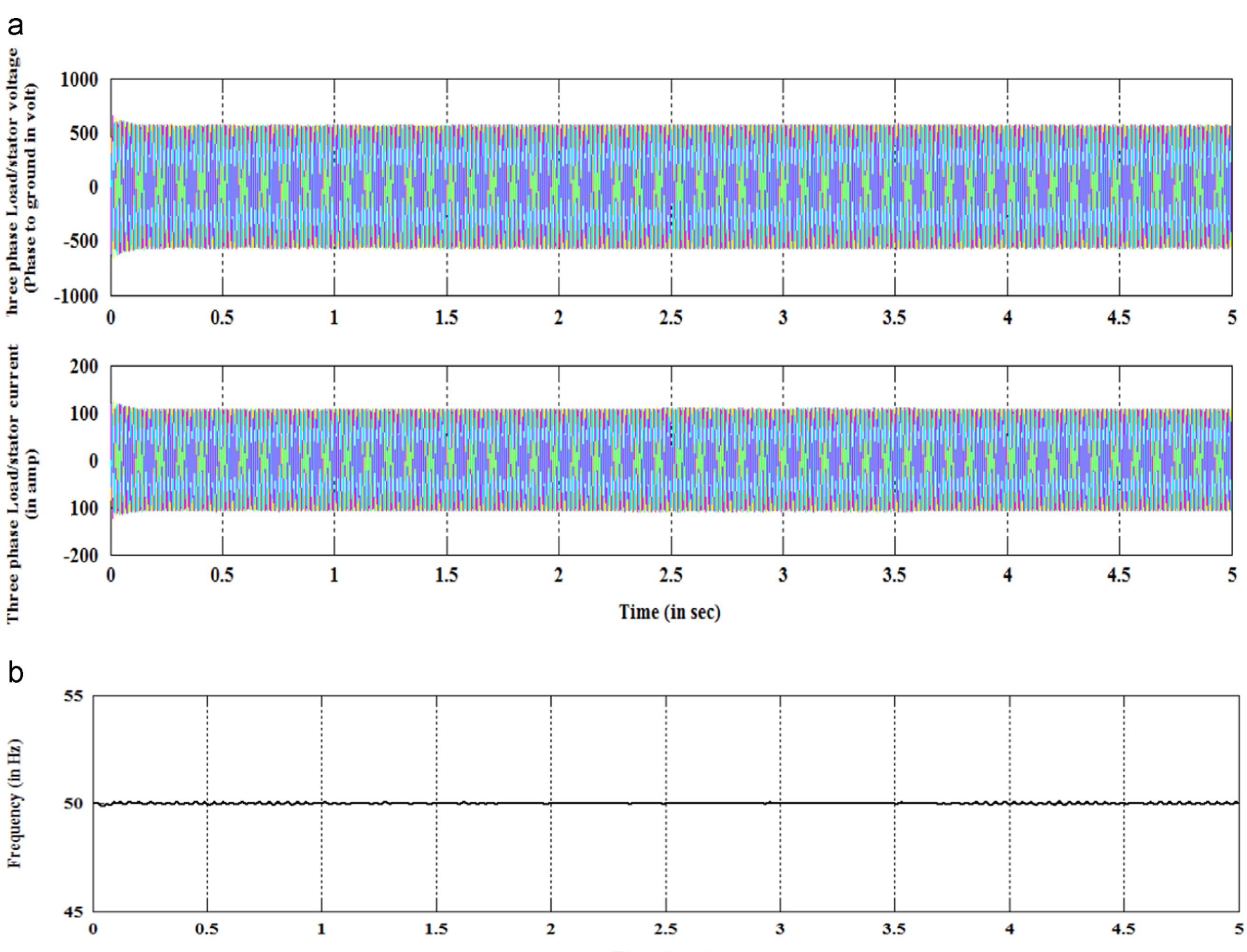


Fig. 22. (a) Load voltage (V_{abc} in volts) and current (I_{abc} in amp) and (b) frequency of stator load/stator voltage.

In Fig. 12(a) load or stator voltage is constant at their reference value i.e. 398.38 V_{rms} (or 563.39 V peak) and also the value of load current and frequency of stator voltage Fig. 12(b) s constant due to constant load.

Both, the active power and reactive power as shown in Fig. 13(a) and (b) respectively, are constant due to constant load. The active power is equal to 90 kW and reactive power is equal to 1 kVAR.

Fig. 14(a) and (b) represents the generator speed and torque. The speed is constant due to the constant wind speed turbine. Torque is also constant due to constant load.

Fig. 15(a) and (b) represents the rotor currents with their enlarged view.

Fig. 16(a) and (b) represents the stator flux and rotor flux in dq reference plan at steady state condition (i.e. constant load and wind speed) respectively. The circular shape of the plots indicates that the generated stator voltage is sinusoidal.

Case 2: Shows the loads switching operation of the system when wind speed is constant. In this case, a load of 30 kW and 0.2 kVAR is connected throughout the simulation i.e. 0–5 s. Another load of 30 kW and 0.2 kVAR connected for the period of 2–4 s and one more load of the same rating is connected for the period of 3–4 s. The results are shown below.

In Fig. 17(a), load or stator voltage (v_{abc}) is constant at their reference value i.e. 398.38 V_{rms} (or 563.39 V peak) but the

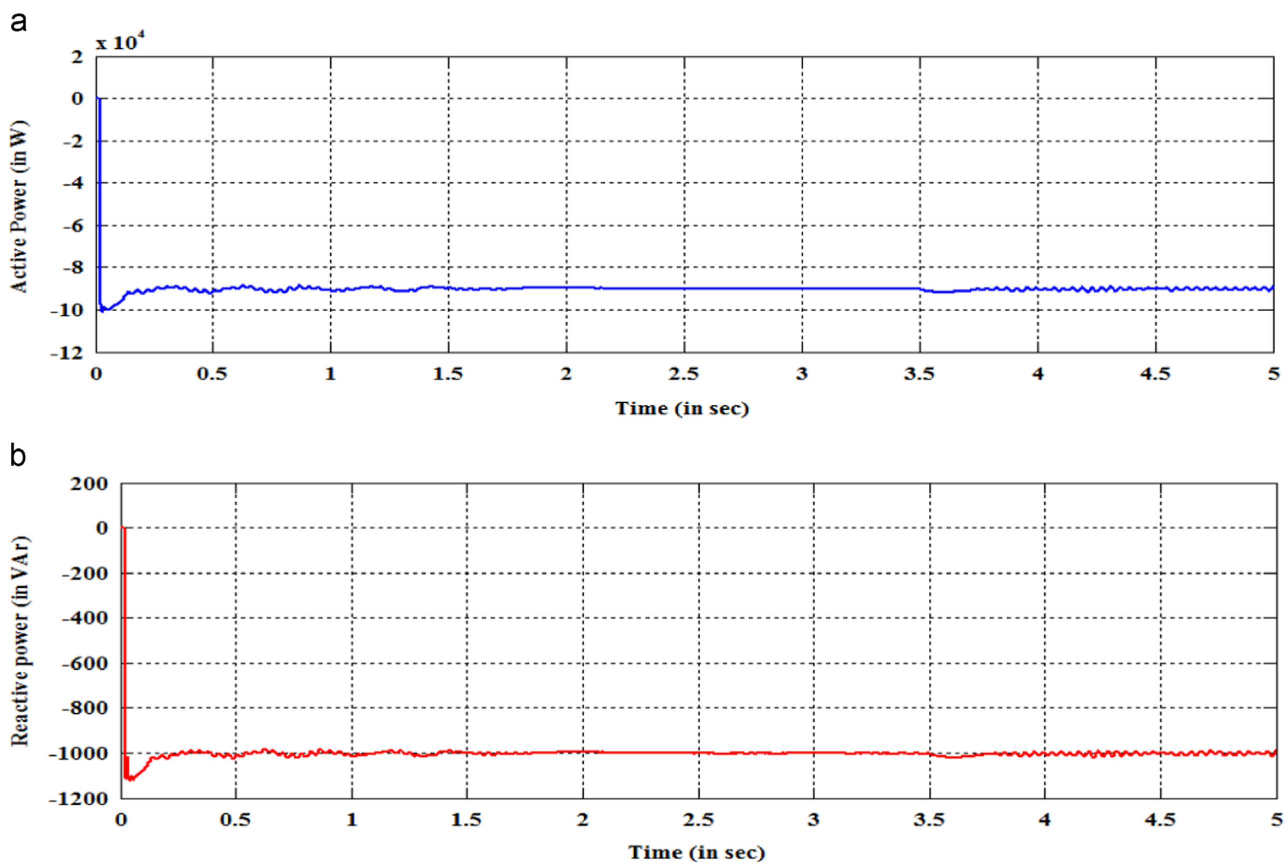


Fig. 23. (a) Active power (in W) and (b) reactive power (in W).

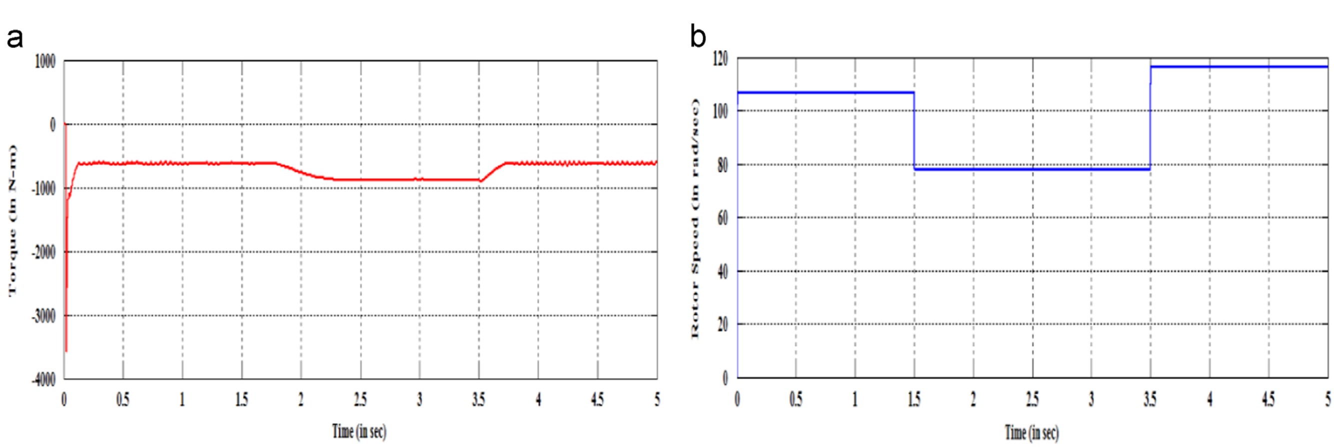


Fig. 24. (a) Generator speed (in rad/s) and (b) Torque (in N m).

current value is changing due to the load switching. The value of current is increased with increase in load and vice-versa. Fig.17(b) shows the enlarged views of (a). Stator/load frequency is shown in Fig. 17(c) and constant at reference value of 50 Hz with very slight variation at the points of the load switching.

In Fig. 18(a), the active power variation is presented. Up to 2 s the active power is equal to 3×10^4 W (i.e. 30 kW). The negative sign shows that the quantity (valid for both active and reactive powers) is delivered from generator (induction motor works as a generator) to the load. Another load is switched ON for a period of 2–4 s, thus the active power is changed to 60 kW from 30 kW. One more load is connected for the period of 3–4 s, thus the active power is changed to 90 kW from 60 kW. After 4 s, the two additional loads are disconnected so that active power retained to its pervious value i.e. 30 kW. Similarly for the reactive power, shown in Fig. 18(b), it is equal to 0.2×10^4 kVAR (i.e. 200 VAr) up to 2 s; 0.4×10^4 kVAR (i.e. 400 VAr) for the period 2–3 s; and 0.6×10^4 kVAR (i.e. 600 VAr) for the period 3–4 s. After 4 s, the two additional loads are disconnected so that reactive power retained to its pervious value i.e. 0.2×210^4 kVAR (i.e. 200 VAr).

Fig. 19(a) and (b) represents the generator speed and torque. The generator speed is constant due to constant wind speed. There is some variation in torque due to variation in load. Negative sign in generator torque shows that it is generator mode and follows the torque supplied by the wind turbine.

Fig. 20(a) and (b) represents the stator flux and rotor flux in dq reference plan respectively. The circular shape of the plots indicates that the generated stator voltage is sinusoidal.

Fig. 21 represents the rotor current variation. There is some variation in rotor current amplitude due to the load switching.

Case 3: In this case, wind speed is variable and load is constant. There is a sudden decrease in wind speed to 8 m/s from 11 m/s at 1.5 s and sudden increase in wind speed to 12 m/s from 8 m/s at 3.5 s. The results are shown below.

In Fig.22(a) load or stator voltage is constant at their reference value i.e. 398.38 V_{rms} (or 563.39 V peak) and also the value of load current and frequency of stator voltage Fig. 22(b) is constant due to constant load.

Both the active power and reactive powers as shown in Fig. 23 (a) and (b) respectively, are constant due to constant load. The active power is equal to 90 kW and reactive power is equal to 1 kVAR.

Fig. 24(a) and (b) represents the generator speed and torque. The speed of generator varies due to the variable wind speed and consequently generator torque also varies.

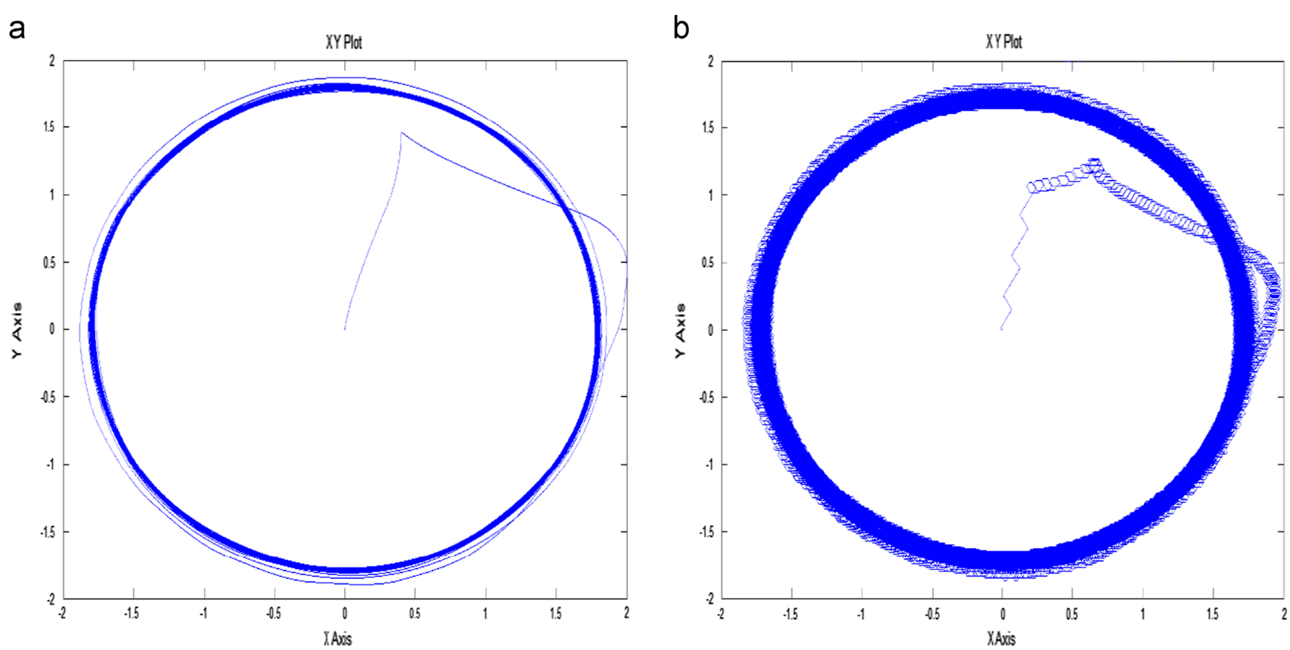


Fig. 25. (a) Rotor flux in d–q plan and (b) stator flux in d–q plan.



Fig. 26. Rotor current (in amp).

Fig. 20(a) and (b) represents the stator flux and rotor flux in dq reference plan respectively when wind is varying and load is constant. The circular shape of the plots indicates that the generated stator voltage is sinusoidal (Fig. 25).

Fig. 26 represents the rotor current variation. There is some variation in rotor current amplitude and frequency due to the variation in wind speed.

Case 4: In this case, the unbalanced load operation the system is shown. The unbalancing in the three phase load of 90 kW and 1 kVAR is created via one phase outing (in between 2 and 4 s) which is worst case of unbalancing. The results are shown below.

In Fig. 27(a) load or stator voltage is constant at their reference value i.e. 398.38 V_{rms} (or 563.39 V peak) and also the value of load current and frequency of stator voltage (Fig. 27(b)) is constant due to constant load. Due to one phase outing of the load, value of the load current in one phase is zero but stator voltage in that phase is maintained at their reference. The current in one phase is zero for the period of 2–4 s but phase voltages are constant at their reference value i.e. 398.38 V_{rms} (or 563.39 V peak).

Fig. 28(a) and (b) represents the generator speed and torque. The speed of generator is constant due to the constant wind speed and generator torque varies because load is varying due to one phase outing. Fig. 28(c) and (b) represents the stator flux and rotor flux in dq reference plan respectively when wind is constant and unbalanced loading. The circular shape of the plots indicates that the generated stator voltage is sinusoidal. Fig. 28(e) represents the rotor current variation. There is some variation in rotor current amplitude due to the variation in load.

5. Conclusion and future scope

In this paper a novel speed sensorless technique for the control of the output voltage and frequency of a DFIG based WECS has been proposed. The proposed control technique is based on rms detection of output voltage. This way an estimation of the rotor speed or position is not required. Using the proposed technique, the stator voltage and frequency are balanced and constant at their reference values. On basis of extensive simulation studies carried out using MATLAB/SIMULINK, it is observed that the performance of the controller both in transient and in steady state is quite satisfactory. Also the simulation results demonstrate that the performance of the controllers is satisfactory under balanced as well as under unbalanced load conditions. A DFIG model based on single phase is described for demonstrating the dependency of stator voltage on rotor currents. The performance of DFIG, in terms of Active power; Reactive power and dc link voltages, was observed when it supplies the isolated (R–L type) load. In addition, a short state-of-the-art review on mechanical position/speed sensorless control schemes for standalone DFIG based WESs is

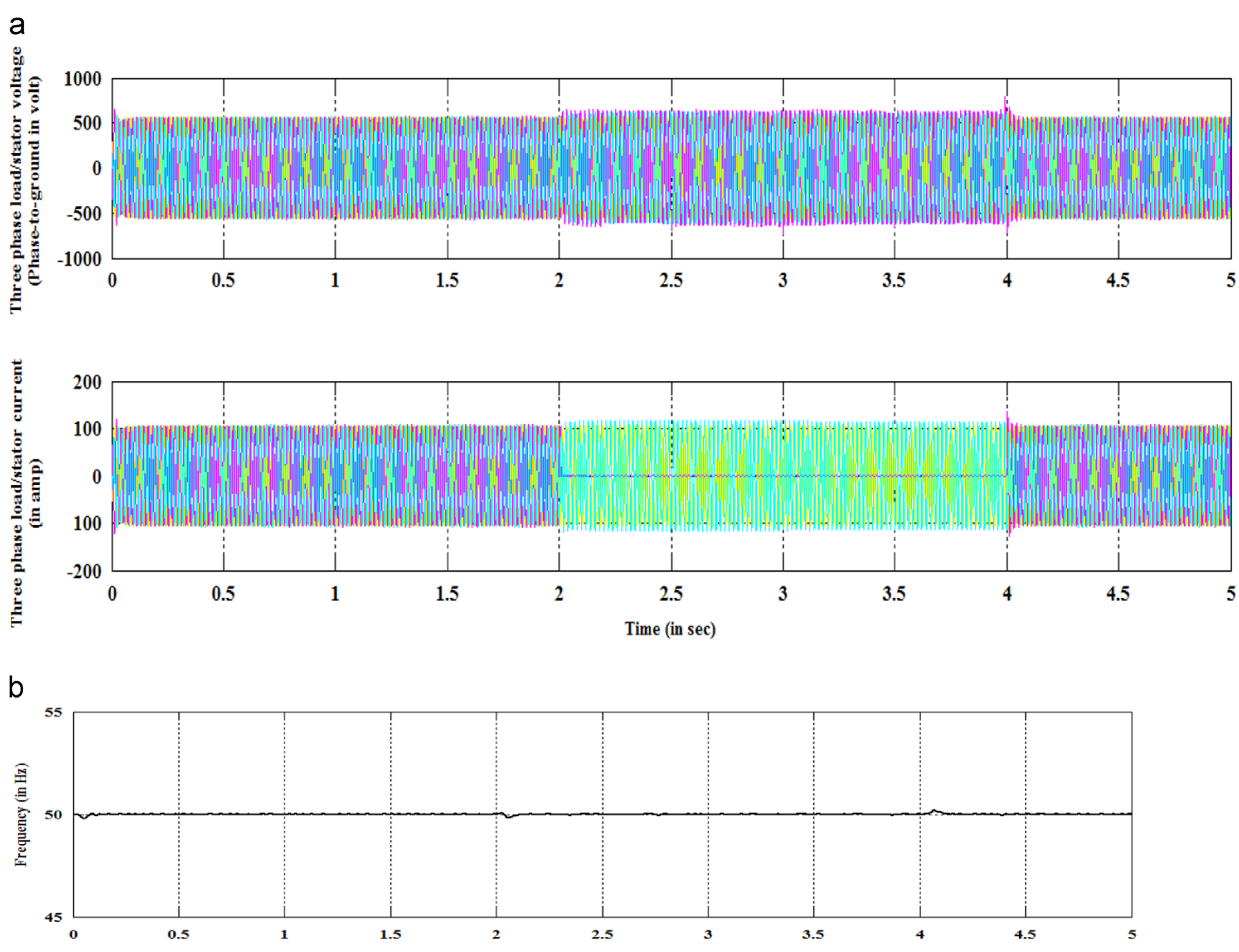


Fig. 27. (a) Load voltage (V_{abc} in volts) and current I_{abc} in amp) and (b) frequency of stator load/stator voltage.

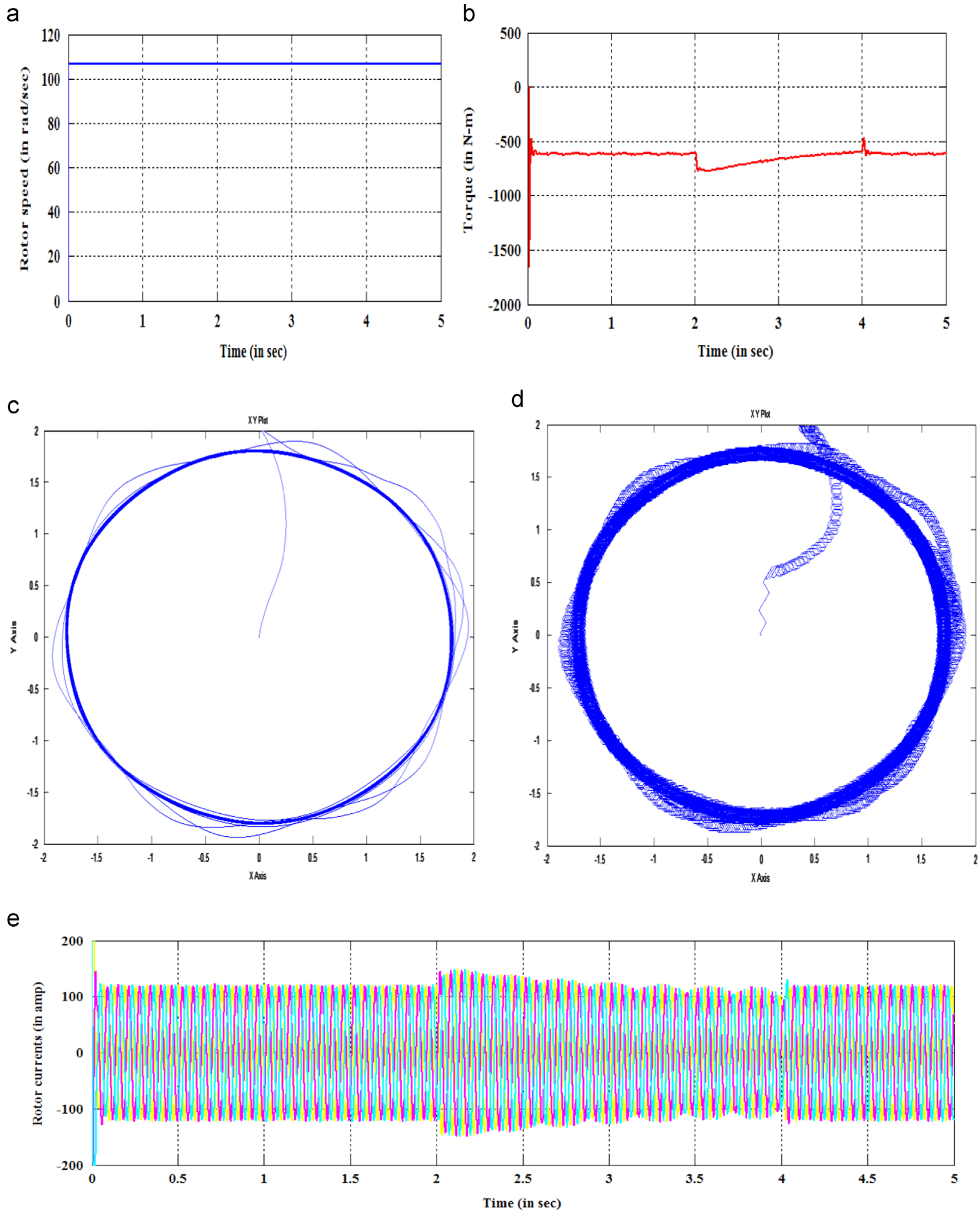


Fig. 28. (a) Load voltage (V_{abc} in volts) and current (I_{abc} in amp) and (b) frequency of stator load/stator voltage.

presented, these include stator flux oriented control techniques; direct voltage control techniques; MARS observer based techniques for autonomous DFIG-based variable-speed WESs. Future work will concern the laboratory tests of the proposed technique in the paper. Also the proposed technique is extending for non-linear loads. Mathematical analysis of controller tuning will be done.

References

[1] Zhe Chen, Guerrero JM, Blaabjerg F. A review of the state of the art of power electronics for wind turbines. IEEE Trans Power Electron 2009;24:1859–73.

[2] Muller S, Deicke M, De Doncker RW. Doubly fed induction generator system for wind turbines. IEEE Ind Appl Mag 2002;8:26–33.

[3] Xu L, Cheng W. Torque and reactive power control of a doubly-fed induction machine by position sensorless scheme. IEEE Trans Ind Appl 1995;31:636–41.
[4] Petersson A, Lundberg S, Thiringer T. A DFIG wind turbine ride-through system. Influence on the energy production. Wind Energy 2005;8:251–63.
[5] Seman S, Niiranen J, Arkkio A. Ride-through analysis o f doubly fed induction wind-power generator under unsymmetrical network disturbance. IEEE Trans Power Syst 2006;21:1782–9.
[6] Carrasco JM, Franquelo LG, Jan T, Bialasiewicz Eduardo G, Guisado RC, Portillo Ma, Prats Ángeles Martín, et al. Power-electronic systems for the grid integration of renewable energy sources: A survey. IEEE Trans. Ind. Electron. 2006;53:1002–16.
[7] Ned Mohan, Brekken Ted KA. Control of a doubly fed induction wind generator under unbalanced grid voltage conditions. IEEE Trans Energy Conver 2007;22 (1):129–35.
[8] Morren Johan, Sjoerd W, de Haan H. Ridethrough of wind turbines with doubly-fed induction generator during a voltage dip. IEEE Trans Energy Conver 2005;20:435–41.
[9] Lopez J, Sanchis Pablo. Dynamic behavior of the doubly fed induction generator during three-phase voltage dips [J]. IEEE Trans Energy Conver 2007;22(3):709–17.
[10] Shukla Rishabh Dev, Tripathi RK. Dynamic performance of DFIG based WECS under different voltage sag. Int J Chemtech Res 2013;5(2):980–92.
[11] Shukla Rishabh Dev, Tripathi RK. Maximum power extraction schemes & power control in wind energy conversion system. Int J Sci Eng Res 2012;3(6).
[12] Pena R, Asher GM, Clare. JC. A doubly fed induction generator using back to back PWM converters supplying an isolated load from a variable speed wind turbine. Proc Inst Elect Eng, Electr Power Appl 1996:380–7.
[13] Jain AK, Ranganathan VT. Wound rotor induction generator with sensorless control and integrated active filter for feeding nonlinear loads in a stand-alone grid. IEEE Trans Ind Electron 2008;55(1):218–28.
[14] Jain Amit Kumar, Ranganathan VT. Wound rotor induction generator with sensorless control and integrated active filter for feeding nonlinear loads in a stand-alone grid. IEEE Trans Ind Electron 2008;55(1).
[15] Poddar G, Ranganathan. VT. Sensorless double-inverter-fed wound-rotor induction-machine drive. IEEE Trans Ind Electron 2006;53:86–95.
[16] Hopfensperger B, Atkinson DJ, Lakin. RA. Stator- flux oriented control of a doubly-fed induction machine without position encoder,. Proc Inst Elect Eng, Electr Power Appl 2000;147(4):241–50.
[17] Goel PK, Singh B, Murthy SS, Kishore N. Modeling and control of autonomous wind energy conversion system with doubly fed induction generator. In: 2010 Joint international conference on power electronics, drives and energy systems (PEDES) & 2010 Power India, New Delhi, India; 20–23 December, 2010.
[18] Iwanski G, Koczara W. Sensorless stand alone variable speed system for distributed generation. In: Proceedings of 35th IEEE PESC. Germany: Aachen; 2004. p. 1915–21.
[19] Iwanski G., Koczara W. Island operation of the variable speed induction generator. In: Proceeedings of 4th IEEE international power electronics and motion control conference, 2004. IPEMC, vol. 2; 2004. p. 896–901.
[20] Iwanski G, Koczara W. Sensorless stand alone variable speed system for distribution generation. In: Proceedings of 2004 IEEE 35th annual power electronics specialists conference, PESC 04, vol. 3; 2004. p. 1915–21.
[21] Iwanski G, Koczara W. Simple autonomous sesnsorless generation system with wound induction machine. IEEE International Symposium on Industrial Electronics, vol. 2; 2004. p. 929–34.
[22] Iwanski G, Koczara W. Controlled and decoupled distributed generation. IEEE Compat Power Electron 2005;2005:18–24.
[23] Iwanski G, Koczara W. Sensorless direct voltage control method for stand-alone slip-ring induction generator. In: Proceedings of 11th EPE, Dresden, Germany, CD-ROM; 2005.
[24] Iwanski G, Koczara W. Positive and negative sequence based sensorless control for stand-alone slip-ring generator. In: Proceedings of 12th EPE-PEMC, Portoroz, Slovenia; 2006. p. 555–60.
[25] Iwanski Grzegorz, Koczara Wlodzimierz. Sensorless direct voltage control of the stand-alone slip-ring induction generator. IEEE Trans Ind Electron 2007;54(2).
[26] Grzegorz Iwanski, Wlodzimierz Koczara. Extended direct voltage control of the stand-alone double fed induction generator. POWERENG2007, Setubal, Portugal; April 12–14, 2007.
[27] Iwanski G, Koczara W. DFIG-based power generation system with UPS function for variable-speed applications. IEEE Trans Ind Electron 2008;55 (8):3047–54.
[28] Iwanski G, Staniak P, Koczara W. Power management in a DC microgrid supported by energy storage. In: Proceedings of IEEE international symposium on industrial electronics (ISIE); 2011. p. 347–52.
[29] Iwanski G. DFIG based standalone power system operating at low load conditions. In: Proceedings of 13th European conference on power electronics and applications, (EPE '09); 2009.
[30] Iwanski G, Koczara W. Rotor current PI controllers in the method of output voltage control of variable speed standalone DFIG. In: Proceedings of 2008 IEEE international symposium on industrial electronics, ISIE; 2008. p. 2450–5.
[31] Iwanski, G. DFIG based power system supplying nonlinear load. In: Proceedings of IEEE 2011 international symposium on industrial electronics (ISIE); 2011. p. 1447–52.
[32] Shukla RD, Tripathi RK. A stand-alone wind energy conversion system using wound rotor induction machine. In: Proceedings of 2013 IEEE international conference on power, energy and control (ICPEC). Sri Rangalatchum Dindigul, Tamilnadu, India; 6–8 February, 2013.
[33] Marcetic DP, Vukosavic SN. Speed-sensorless AC drives with the rotor time constant parameter update. IEEE Trans Ind Electron 2007;54(5):2618–25.
[34] Comanescu M, Xu L. Sliding-mode MRAS speed estimators for sensor-less vector control of induction machine. IEEE Trans Ind Electron 2005;53 (1):146–53.
[35] Pena RS, Cardenas RJ, Asler GM, Clare JC. Vector controlled induction machines for stand-alone wind energy applications. Ind Appl Conf 2000;3:1409–15.
[36] Cardenas R, Pena R, Proboste J, Asher G, Clare. J. MRAS observer for sensorless control of standalone doubly fed induction generators. IEEE Trans Energy Convers 2005;20(4):710–8.
[37] Cárdenas Roberto, Peña Rubén, Proboste José, Asher Greg, Clare Jon. MRAS observer for sensorless control of standalone doubly fed induction generators. IEEE Trans Energy Convers 2005;20(4):710–8.
[38] Cardenas RJ, Pena RS, Proboste J, Asher GM, Clare JC. Sensorless control of doubly fed induction Generator for standalone. In: Proceedings of 35th annual IEEE power electronics specialist conference, PESC'04; 2004.
[39] JinWen G, XuHui W. Research on a novel motor flux observer based on voltage model. In: Proceedings of 10th IEEE international power electronics conference, CIEP, Puebla, Mexico; October 2006. p. 1–5.
[40] Cárdenas R, Peña RS, Asher G, Clare J, Cartes J. MRAS observer for doubly fed induction machines. IEEE Trans. Energy Convers 2004;19(2):467–8.
[41] Peña RS, Cardenas R, Proboste J, Asher G, Clare J. Sensorless control of a slip ring induction generator based on rotor current MRAS observer. In: Proceedings of 36th IEEE PESC; June 2005. p. 2508–13.
[42] Cardenas R, Peña R, Proboste J, Asher G, Clare J. Rotor current based MRAS observer for doubly-fed induction machines. Electron Lett 2004;40(12): 769–70.
[43] Forchetti DG, Solsona JA, Garcıa GO, Valla. MI. A control strategy for stand-alone wound rotor induction machine. Electr Power Syst Res 2007;77:163–9.
[44] Forchetti Daniel G, García Guillermo O, Inés Valla María. Adaptive observer for sensorless control of stand-alone doubly fed induction generator. IEEE Trans Ind Electron 2009;56:4174–80.
[45] Peña Rubén, Cárdenas Roberto, Proboste José, Asher Greg, Clare Jon. Sensorless control of doubly-fed induction generators using a rotor-current-based MRAS observer. IEEE Trans Ind Electro 2008;55(1).
[46] Pattnaik M, Kastha D. Comparison of MRAS based speed estimation methods for a stand alone doubly fed induction generator. In: Proceedings of 2011 international conference on energy, automation, and signal (ICEAS); 2011. p. 1–6.
[47] Pattnaik MP, Kastha DK. Reactive power based MARS observer for speed sensorless control of double output induction generator. In: Proceedings of IEEE international conference on industrial and information systems (ICIIS); 2010. p. 556–61.
[48] Forchetti DG, Solsona JA, Garc´ıa GO, Valla MI. A control strategy for stand-alone wound rotor induction machine 2007163–9Electr Power Syst Res 2007;77:163–9.
[49] Verghese GC, Sanders SR. Observers for flux estimation in induction machines. IEEE Trans Ind Electron 1998;35(1):85–94.
[50] Morel L, Godfroid H, Mirzaian A, Kauffmann. JM. Double-fed induction machine: converter optimization and field oriented control without position sensor. Proc Inst Elect Eng, Electr Power Appl 1998;145(4):360–8.
[51] Bogalecka E, Krzeminski Z. Sensorless control of a double-fed machine for wind power generators. In: Proceedings of European Conference on Power Electronics, Machines Control, Dubrovnik and Cavtat, Slovenia; 2002.
[52] Forchetti D, Solsona JA, Garcia GO, Valla MI. A control strategy for stand-alone wound rotor induction machine. Elect Power Syst Res 2007;77(2):163–9.
[53] Abad Gonzalo, Lopez Jesus, Rodriguez Miguel, Marroyo Luis, Iwanski Grzegorz. Double fed induction machine-modeling and control for wind energy generation. IEEE Press Series on Power Engineering. Canada: Wiley Publication; 2011.
[54] Yazdani A. Islanded operation of a doubly fed induction generator (DFIG) wind-power system with integrated energy storage. In: Proceedings of Electrical power conference, 2007. EPC 2007. IEEE, Canada; 2007. p. 153–9.
[55] El-helw HM, Tennakoon SB. Vector control of a doubly fed induction generator for standalone wind energy application. Wind power to the grid – EPE wind energy, Chapter 1st Seminar, 2008. EPE-WECS; 2008.
[56] Bhuiyan FA, Yazdani A. Mutlimode, control of a DFIG-based wind power unit for remote applications. IEEE Trans Power Deliv 2009;24(4):2079–89.
[57] Phan Van-Tung, Lee Hong-Hee. Performance enhancement od stand-alone DFIG systems with control of rotor and load side converters using resonant controllers. IEEE Trans Ind Appl 2012;48(1):199–210.
[58] Zhang Chun-jiang, Chai Xiu-Hui, Du-Cui, Wang Hui, Zang Xun. The islanding start and operation control of doubly fed wind generation system. In: Proceedings of 2012 7th IEEE international power electronics and motion control conference (IPEMC), Chain; June 2–5, 2012.
[59] Phan Van-Tung, Kwak Sung-Hyo, LeeHong-Hee. An improved control method for DFIG-based wind system supplying unbalanced stand-alone loads. In: Proceedings of IEEE international symposium on industrial electronics. ISIE 2009 Seoul Olympic Parktel, Seoul, Korea; July 5–8, 2009.
[60] Chu H-Y, Jou H-L, Huang C-L. Transient response of a peak voltage detector for sinusoidal signals. IEEE Trans Ind Electron 1992;39:74–9.